Finite element formulation of metal foam microbeams via modified strain gradient theory

Armagan Karamanli[a,*], Thuc P. Vo[b], Omer Civalek[c]

[a] Faculty of Engineering and Natural Sciences, Mechanical Engineering, Istinye University, Istanbul, Turkey.

[b] School of Engineering and Mathematical Sciences, La Trobe University, Bundoora, VIC 3086, Australia

[c] Research Center for Interneural Computing, China Medical University, 40402, Taichung, Taiwan

[*]Corresponding author. E-mail: armagan.karamanli@istinye.edu.tr (A. Karamanli)

Abstract

Size-dependent behaviours of metal foam microbeams with three different porosity distribution models are studied in this paper. Based on finite element model, a normal and shear deformation theory has been employed for the first time to investigate their structural behaviours by using modified strain gradient theory and considering the effects of variable material length scale parameter. The equations of motion and boundary conditions of system are derived from Hamilton's principle. Finite element models are presented for the computation of deflections, vibration frequencies and buckling loads of the metal foam microbeams. The verification of proposed models is carried out with comparison of the numerical results available in the literature. Calculations using the different parameters reveal the effects of the porosity parameters (distribution and coefficient), small size, boundary conditions and Poisson's ratio on the displacements, frequencies and buckling loads of metal foam microbeams. Some benchmark results of these structures for both models (modified couple stress theory and modified strain gradient theory with constant and variable material length scale parameter) and with/without Poison's effect are provided for future study.

Keywords: Gradient elasticity, metal foam microbeams, variable material length scale parameter

Nomenclature

IGA	Iso-geometric analysis	$\sigma_{ij}, m_{ij}, p_i, \tau_{ijk}$	Stress and modified strain gradient stress components
FSDT	First order shear deformation theory	$\varepsilon_{ij}, \chi_{ij}, \gamma_i, \eta_{ijk}$	Strain and symmetric curvature, dilatation gradient and deviatoric stretch gradient tensors
CST	Classical shell theory	u_1, u_2, u_3	Displacements in the 1,2 and 3 directions of an arbitrary point
CCT	Classical continuum theory	δ_{ij}	Kronecker delta
MCST	Modified couple stress theory	e_{ijk}	Permutation symbol
MSGT	Modified strain gradient theory	ν	Poisson's ratio
NSGT	Nonlocal strain gradient theory	$\mathcal{V}$	Volume of the body, which can be decomposed to the cross-sectional area $A = bxh$ and the length of the domain *L*
CNT	Carbon nanotube	ℓ_0, ℓ_1 and ℓ_2	MLSPs of modified stress tensors
MLSP	Material length scale parameter	u, w_b, w_s and w_z	In plane displacement and bending, shear and thickness stretching displacements
NSDT	Normal and shear deformation theory	$f_1(z), f_2(z)$ and $f_3(z)$	Shape function describing the contribution of the bending, shear and thickness stretching displacements across the thickness
FEM	Finite element method	TBT	Third order beam theory
L, b, h	Geometry of beam	Q_{ij}	Elastic constants
UPD	Uniform porosity distribution	q	Uniformly distributed load
NUPD1	Non-uniform porosity distribution 1	N_0	Axial load
NUPD2	Non-uniform porosity distribution 2	$I_0, I_1, I_2, J_1, J_2, J_3, K_1, K_2$	Inertial constant coefficients
E	Young's modulus	ω	Natural frequency
ρ	Mass density	φ_j	FEM shape function
ℓ	MLSP	Π	Total energy
E_{max}	Maximum *E*	$[K_{kl}]$, $[M_{kl}]$, $[G_{kl}]$ and F_k	FEM matrices
E_{min}	Minimum *E*	BC	Boundary condition
ρ_{max}	Maximum ρ	DMD ($\overline{w}$)	Dimensionless mid-span deflection
e_0	Porosity parameter	DFF ($\bar{\lambda}$)	Dimensionless fundamental frequency
e_m	Porosity parameter	DCBL ($\overline{N}_{cr}$)	Dimensionless critical buckling load
ℓ_{max}	Maximum MLSP	SBT	Sinusoidal beam theory
$\mathcal{U}, V, K$	Strain energy, external work and kinetic energy		

1. Introduction

In recent years, the stringent norms raised to achieve zero carbon emissions accompanied with low fuel consumption are directly effecting the engineering applications especially in the automotive and aerospace industries. As a result, the usage of parts manufactured by using the cellular lightweight materials has been increasing due to their outstanding mechanical and thermal properties. Metal foams have the high stiffness to weight ratio, impact and energy absorption, higher structural damping capacity than the solids, sound and vibration isolation, better thermal conductivity due to high surface area and greater cell wall conduction. Moreover, the exhibition of plateau stress can also be observed in metal foam structures [1]. Because of these manifold features of metal foam, researchers have been working on the comprehensive studies for improving and optimizing the mechanical responses of these structural members, which are the beams, plates and shells.

The flexural and stability behaviours of a simply supported isotropic beams with porosity employing a finite element model [2, 3] and sandwich beams with a porous core using Navier's method [4] are studied. Elasto-static bending and buckling responses of Timoshenko metal foam beam are studied based on Ritz method [5]. Natural frequency and transient analysis of metal foam beams are investigated using Ritz and Newmark-β methods [6]. Nonlinear Timoshenko beam model is developed to investigate natural frequencies of sandwich beams with metal foam core [7]. The Ritz method is employed to understand the elastic stability and natural frequencies of graphene platelets reinforced Timoshenko metal foam [8]. Nonlinear dynamic stability of metal foam beams is presented [9]. Dynamic responses of Timoshenko metal foam single and multi-span beams are presented for flexible end conditions [10]. A new method is developed to study the nondeterministic dynamic responses of Timoshenko metal foam beams [11]. Various boundary conditions including the flexible ones, the natural frequencies of higher order shear deformable metal foam beams are investigated [12]. A normal and shear deformation theory is used to investigate the vibration and elastic bending

of the metal foam beams based on iso-geometric analysis (IGA) [13]. Mechanical behaviours of graphene foam beams are presented by implementing Rayleigh-Ritz method [14]. An optimization study is performed for the stability response of beams having functionally graded faces and metal foam core [15].

Elasto-static bending and stability behaviours of simply supported metal foam plate are presented in [16]. Navier solutions based on the stability analysis are provided for the simply support sandwich plate with metal foam core [17]. Differential quadrature technique is implemented to obtain the numerical results for the free vibrations of the third order shear deformable metal foam plate [18]. Nonlinear classical plate theory is applied to obtain free vibration response of the metal foam plates reinforced by graphene platelets [19]. The dynamic responses of sandwich metal foam plate with a viscoelastic core based on the modified Fouirer – Ritz method are investigated by implementing a first order shear deformation theory (FSDT) [20]. Natural frequency response of the elastically founded metal foam plates are studied [21].

Analytical nonlinear dynamical solutions are presented based on the FSDT by employing thermal effects for the metal foam truncated conical panel [22]. Ballistic capacity of the sandwich panels having porous core is studied [23]. Employing the nonlinear classical shell theory (CST) and Navier's method, resonance behaviours of metal foam cylindrical shells are investigated [24]. The Ritz method and FSDT are implemented to investigate the free vibration responses of metal foam cylindrical, spherical and shallow shells for different end conditions [25-29]. Analytical solutions based on the nonlinear CST are obtained to present the bending and hygrothermal stability behaviours of metal foam cylindrical shells [30]. The nonlinear CST is employed to analyse the stability of the metal foam cylindrical shells [31]. The FSDT is used to study the wave propagations in the cylindrical metal foam shells rested on a variable elastic foundation [32]. Functionally graded electromagnetic layers are used for controlling the vibration behaviours of rotating cylindrical shells with a metal foam core and

nanocomposite faces [33]. A comprehensive review based on the structural behaviours of metal foam structures can be found in [34].

Although many papers are carried out to investigate structural responses of metal foams for macroscale structures (beams/plates/shells) using the classical continuum theory (CCT), there is still limit research on small-scale ones. In order to capture size effects in these structures, higher-order continuum models such as modified couple stress theory (MCST [35]) and modified strain gradient theory (MSGT [36]), nonlocal theory [37], nonlocal strain gradient theory (NSGT [38]), etc. can be used. Nonlocal wave propagation of porous nanobeam is studied using the Euler-Bernoulli and Timoshenko beam theories [39]. Navier's method is implemented to analyse the vibrations of sandwich beams having carbon nanotube (CNT) reinforced faces with metal foam core with MCST [40] and simply-supported metal foam beams with MSGT [41]. Post-buckling of metal foam simply-supported microbeams with variable material length scale parameter (MLSP) is investigated by MCST and Euler–Bernoulli theory [42]. Under periodic excitation, the vibration responses of silicon foam nanobeams are examined via surface elasticity theory [43]. IGA is used to present the nonlinear flexural responses of metal foam plate with NSGT [44]. An exponential plate theory is employed to study the linear and nonlinear vibration behaviours of axially loaded strain gradient metal foam graphene platelets reinforced microplates [45]. The vibration characteristics of CNT reinforced metal foam microplates are investigated under the hygrothermal effects by using a trigonometric plate theory [46]. The forced vibration analysis of NSGT metal foam nanoshells is revealed by employing the FSDT [47]. Free vibrations of cylindrical nanoshells metal foam are investigated using MCST and Love's thin shell theory [48]. Using the FSDT, wave propagations of nonlocal strain gradient graphene platelets reinforced metal foam nanoshells are examined considering the thermal effects [49]. The FSDT with MCST is employed to study vibration behaviours of rotating metal foam

truncated sandwich conical micro-shells having graphene-platelets faces [71]. Some important studies based on nonlocal elasticity can be found in Refs. [56-70, 72-74].

Based on the open literature investigation provided above, and to the best of authors' knowledge, the structural behaviours of metal foam microbeams based on NSDT, MSGT and finite element model (FEM) is not available. Moreover, the effects of variable MLSP on their responses have not been investigated yet. This is complicated problems and thus needs further investigation to fill the gap. That is the main novelty and contribution of this study. To achieve this, FEM is developed to investigate the elastic bending, natural frequency and stability responses of metal foam microbeams using NSDT based on the CCT, MCST and MSGT. The effects of boundary conditions, aspect ratios, porosity variations, thickness to MLSP ratios and Poisson's ratio on the structural responses of the metal foam microbeams are presented. The necessary of including three MLSPs in the MSGT rather than only in the MCST and effects of variable MLSP on the responses of metal foam microbeams are discussed in details.

2. Theoretical Formulation of Metal Foam Microbeams

By using the Cartesian coordinate system, the geometry of a metal foam beam with length (L), width (b) and height (h) can be visualized in Fig.1. Within the study, various metal foam models in terms of the different distribution of porosity are presented, namely, uniformly (UPD), non-uniformly 1 (NUPD1) and non-uniformly 2 (NUPD2). The distribution of the porosities is symmetric in NUPD1 according to mid-plane, however, it is asymmetric in NUPD2. The Young's modulus (E), mass density (ρ) and MLSP (ℓ) of the metal foam models can be given by [5-10]:

UPD:

$$E(z) = E_{max}(1 - e_0\Lambda) \tag{1a}$$

$$\rho(z) = \rho_{max}\sqrt{1 - e_0\Lambda} \tag{1b}$$

$$\ell(z) = \ell_{max}\sqrt{1 - e_0\Lambda} \tag{1c}$$

$$\Lambda = \frac{1}{e_0} - \frac{1}{e_0}\left(\frac{2}{\pi}\sqrt{1 - e_0} - \frac{2}{\pi} + 1\right)^2 \tag{1d}$$

NUPD1:

$$E(z) = E_{max}\left[1 - e_0 cos\left(\frac{\pi z}{h}\right)\right] \tag{2a}$$

$$\rho(z) = \rho_{max}\left[1 - e_m cos\left(\frac{\pi z}{h}\right)\right] \tag{2b}$$

$$\ell(z) = \ell_{max}\left[1 - e_0 cos\left(\frac{\pi z}{h}\right)\right] \tag{2c}$$

NUPD2:

$$E(z) = E_{max}\left[1 - e_0 cos\left(\frac{\pi z}{2h} + \frac{\pi}{4}\right)\right] \tag{3a}$$

$$\rho(z) = \rho_{max}\left[1 - e_m cos\left(\frac{\pi z}{2h} + \frac{\pi}{4}\right)\right] \tag{3b}$$

$$\ell(z) = \ell_{max}\left[1 - e_0 cos\left(\frac{\pi z}{2h} + \frac{\pi}{4}\right)\right] \tag{3c}$$

where E_{max} and ρ_{max} indicates the maximum E and ρ values, respectively; e_0 and e_m refer the porosity parameters for E and ρ, and can be calculated by using the following equations [5-10]:

$$e_0 = 1 - \frac{E_{min}}{E_{max}} \tag{4a}$$

$$e_m = 1 - \sqrt{1 - e_0} \tag{4b}$$

where E_{min} is the minimum value of E. It is noted that e_0 is used to control the porosity volume fraction within this study.

In order to develop the FEM model for the metal foam microbeams, the strain energy ($\mathcal{U}$) can be revealed by [36, 50-52]:

$$\mathcal{U} = \frac{1}{2}\int_{V} \left(\sigma_{ij}\varepsilon_{ij} + m_{ij}\chi_{ij} + p_i\gamma_i + \tau_{ijk}\eta_{ijk}\right) d\mathcal{V}, \quad i,j,k = 1,2,3 \tag{5}$$

where σ_{ij}, m_{ij}, p_i and τ_{ijk} represent the classical stress and modified stress tensors, respectively and ε_{ij}, χ_{ij}, γ_i and η_{ijk} are the classical strain, symmetric curvature, dilatation gradient and deviatoric stretch gradient tensors, respectively.

If one uses the displacement field (u_1, u_2, u_3), then the components of the classical and modified strain tensors can be obtained as [36, 50-52]:

$$\varepsilon_{ij} = \frac{1}{2}\left(\frac{\partial u_i}{\partial x_j} + \frac{\partial u_j}{\partial x_i}\right) \tag{6a}$$

$$\chi_{ij} = \frac{1}{4}\left(e_{imn}\frac{\partial^2 u_n}{\partial x_{mj}^2} + e_{jmn}\frac{\partial^2 u_n}{\partial x_{mi}^2}\right) \tag{6b}$$

$$\gamma_i = \frac{\partial \varepsilon_{mm}}{\partial x_i} \tag{6c}$$

$$\eta_{ijk} = \frac{1}{3}\left(\frac{\partial \varepsilon_{jk}}{\partial x_i} + \frac{\partial \varepsilon_{ki}}{\partial x_j} + \frac{\partial \varepsilon_{ij}}{\partial x_k}\right) - \frac{1}{15}\left[\delta_{ij}\left(\frac{\partial \varepsilon_{mm}}{\partial x_k} + 2\frac{\partial \varepsilon_{mk}}{\partial x_m}\right) + \delta_{jk}\left(\frac{\partial \varepsilon_{mm}}{\partial x_i} + 2\frac{\partial \varepsilon_{mi}}{\partial x_m}\right) + \delta_{ki}\left(\frac{\partial \varepsilon_{mm}}{\partial x_j} + 2\frac{\partial \varepsilon_{mj}}{\partial x_m}\right)\right] \tag{6d}$$

where δ_{ij} and e_{ijk} state the Kronecker delta and permutation symbol.

Constitutive relations are depicted by using the modified stress tensors and Poisson's effect for a linear elastic metal foam beam as [36, 50-52]:

$$\sigma_{ij} = \left(\frac{E(z)}{1+\nu}\right)\varepsilon_{ij} + \left[\frac{\nu E(z)}{(1+\nu)(1-2\nu)}\right]\varepsilon_{kk}\delta_{ij} \tag{7a}$$

$$p_i = \left(\frac{E(z){\ell_0}^2(z)}{1+\nu}\right)\gamma_i \tag{7b}$$

$$\tau_{ijk} = \left(\frac{E(z){\ell_1}^2(z)}{1+\nu}\right)\eta_{ijk} \tag{7c}$$

$$m_{ij} = \left(\frac{E(z){\ell_2}^2(z)}{1+\nu}\right)\chi_{ij} \tag{7d}$$

where ℓ_0, ℓ_1 and ℓ_2 can be the associated MLSPs of modified stress tensors. If one sets $\ell_0 = \ell_1 = 0$, the MCST formulation is obtained. By setting the MLSP to zero, the CCT formulation is derived.

The displacement field of NSDT used for the numerical computations can be provided in the form of [50, 51, 53, 54]:

$$u_1(x,z,t) = U(x,z,t) = u(x,t) - f_1(z)\frac{\partial w_b(x,t)}{\partial x} + f_2(z)\frac{\partial w_s(x,t)}{\partial x} \tag{8a}$$

$$u_3(x,t) = W(x,t) = w_b(x,t) + w_s(x,t) + f_3(z)\, w_z(x,t) \tag{8b}$$

$$f_1(z) = \frac{4z^3}{3h^2}, f_2(z) = z - \frac{8z^3}{3h^2} \;\; and \;\; f_3(z) = 1 - \frac{4z^2}{h^2} \tag{8c}$$

where $u, w_b, w_s \; and \; w_z$ are the components of in-plane and transverse displacements, respectively. If one sets the $f_3(z) = 0$, then a third order beam theory (TBT) formulation is obtained.

The classical and modified strains can be revealed based on the employed NSDT by:

$$\varepsilon_x = \frac{\partial U}{\partial x} = u' - f_1 w_b'' + f_2 w_s'' \tag{9a}$$

$$\varepsilon_z = \frac{\partial W}{\partial z} = f_3{}' w_z \tag{9b}$$

$$\varepsilon_{xz} = \frac{\gamma_{xz}}{2} = \frac{\partial W}{\partial x} + \frac{\partial U}{\partial z} = \frac{1}{2} f_3 (w_b' + 2w_s' + w_z') \tag{9c}$$

$$\chi_{xy} = \frac{1}{4}[-(1 + f_1{}')w_b'' - (1 - f_2{}')w_s'' - f_3 w_z''] \tag{9d}$$

$$\chi_{yz} = \frac{1}{2}\left(\frac{\partial \theta_z}{\partial y} + \frac{\partial \theta_y}{\partial z}\right) = \frac{1}{4}(-f_1{}'' w_b' + f_2{}'' w_s' - f_3{}' w_z') \tag{9e}$$

$$\gamma_x = u'' - f_1 w_b''' + f_2 w_s''' + f_3{}' w_z' \tag{9f}$$

$$\gamma_z = -f_1{}' w_b'' + f_2{}' w_s'' + f_3{}'' w_z \tag{9g}$$

$$\eta_{xxx} = \frac{1}{5}[2u'' - 2f_1 w_b''' - f_3{}' w_b' + 2f_2 w_s''' - 2f_3{}' w_s' - f_3{}' w_z'] \tag{9h}$$

$$\eta_{zzz} = \frac{1}{5}[f_1{}' w_b'' - f_3 w_b'' - f_2{}' w_s'' - 2f_3 w_s'' + 2f_3{}'' w_z - f_3 w_z''] \tag{9i}$$

$$\eta_{yyx} = \eta_{yxy} = \eta_{xyy} = \frac{1}{15}[-3u'' + 3f_1 w_b''' - f_3{}' w_b' - 3f_2 w_s''' - 2f_3{}' w_s' - 2f_3{}' w_z'] \tag{9j}$$

$$\eta_{zzx} = \eta_{zxz} = \eta_{xzz} = \frac{1}{15}[-3u'' + 3f_1 w_b''' + 4f_3{}' w_b' - 3f_2 w_s''' + 8f_3{}' w_s' + 8f_3{}' w_z'] \tag{9k}$$

$$\eta_{xxz} = \eta_{xzx} = \eta_{zxx} = \frac{1}{15}[-4f_1{}' w_b'' + 4f_3 w_b'' + 8f_3 w_s'' + 4f_2{}' w_s'' + 4f_3 w_z'' - 3f_3{}'' w_z] \tag{9l}$$

$$\eta_{yyz} = \eta_{yzy} = \eta_{zyy} = \frac{1}{15}[f_1{}' w_b'' - f_3 w_b'' - f_2{}' w_s'' - 2f_3 w_s'' - 3f_3{}'' w_z - f_3 w_z''] \tag{9m}$$

$$\chi_{xx} = \chi_{yy} = \chi_{zz} = \chi_{xz} = \gamma_y = \eta_{zzy} = \eta_{zyz} = \eta_{yzz} = \eta_{yyy} = \eta_{xyz} = \eta_{yzx} = \eta_{zxy} = \eta_{xzy}$$
$$= \eta_{zyx} = \eta_{yxz} = 0 \qquad (9n)$$

The detailed formulations of classical and modified strain tensors based on the employed NSDT can be found in [50-52].

The stress-strain relations for metal foam microbeams can be noted by:

$$\begin{Bmatrix} \sigma_x \\ \sigma_z \\ \sigma_{xz} \end{Bmatrix} = \begin{bmatrix} Q_{11} & Q_{13} & 0 \\ Q_{13} & Q_{33} & 0 \\ 0 & 0 & Q_{44} \end{bmatrix} \begin{Bmatrix} \varepsilon_x \\ \varepsilon_z \\ 2\varepsilon_{xz} \end{Bmatrix} \qquad (10a)$$

$$Q_{11}(z) = Q_{33}(z) = \frac{E(z)(1-v)}{(1-2v)(1+v)} \text{ with Poisson's effect} \qquad (10b)$$

$$Q_{13}(z) = \frac{vE(z)}{(1-2v)(1+v)} \text{ with Poisson's effect} \qquad (10c)$$

$$Q_{11}(z) = Q_{33}(z) = \frac{E(z)}{1-v^2} \text{ without Poisson's effect} \qquad (10d)$$

$$Q_{13}(z) = \frac{vE(z)}{1-v^2} \text{ without Poisson's effect} \qquad (10e)$$

$$Q_{44}(z) = \frac{E(z)}{2(1+v)} \qquad (10f)$$

$$\begin{Bmatrix} p_x \\ p_z \end{Bmatrix} = \frac{E(z){\ell_0}^2(z)}{1+\nu} \begin{Bmatrix} \gamma_x \\ \gamma_z \end{Bmatrix} \qquad (10g)$$

$$\begin{Bmatrix} \tau_{xxx} \\ \tau_{zzz} \\ \tau_{xyy} \\ \tau_{xzz} \\ \tau_{zxx} \\ \tau_{zyy} \end{Bmatrix} = \frac{E(z){\ell_1}^2(z)}{1+\nu} \begin{Bmatrix} \eta_{xxx} \\ \eta_{zzz} \\ \eta_{xyy} \\ \eta_{xzz} \\ \eta_{zxx} \\ \eta_{zyy} \end{Bmatrix} \qquad (10h)$$

$$\begin{Bmatrix} m_{xy} \\ m_{yz} \end{Bmatrix} = \frac{E(z){\ell_2}^2(z)}{1+\nu} \begin{Bmatrix} \chi_{xy} \\ \chi_{yz} \end{Bmatrix} \qquad (10i)$$

Based on the displacement field of NSDT, the strain energy ($\mathcal{U}$) of the metal foam microbeams can be depicted by:

$$\mathcal{U} = \frac{1}{2}\int_V \Big[(Q_{11}{\varepsilon_x}^2 + 2Q_{13}\varepsilon_x\varepsilon_z + Q_{11}{\varepsilon_z}^2 + Q_{44}{\gamma_{xz}}^2) + \frac{E{\ell_0}^2}{1+\nu}({\gamma_x}^2 + {\gamma_z}^2) + \frac{E{\ell_1}^2}{1+\nu}({\eta_{xxx}}^2 + {\eta_{zzz}}^2 + 3{\eta_{xyy}}^2 + 3{\eta_{xzz}}^2 + 3{\eta_{zxx}}^2 + 3{\eta_{zyy}}^2) + \frac{E{\ell_2}^2}{1+\nu}\left(2{\chi_{xy}}^2 + 2{\chi_{yz}}^2\right)\Big] dV \quad (11)$$

The potential energy of the uniformly distributed load q, axial load N_0 and kinetic energy of metal foam microbeams are presented by:

$$V = -\frac{1}{2}\int_0^L N_0\left\{\left(\frac{\partial w_b}{\partial x}\right)^2 + \left(\frac{\partial w_s}{\partial x}\right)^2 + \left(\frac{\partial w_z}{\partial x}\right)^2 + 2\frac{\partial w_b}{\partial x}\frac{\partial w_s}{\partial x} + 2\frac{\partial w_b}{\partial x}\frac{\partial w_z}{\partial x} + +2\frac{\partial w_s}{\partial x}\frac{\partial w_z}{\partial x}\right\} dx - \int_0^L \{q(w_b + w_s + f_3(z)w_z\} dx \quad (12)$$

$$K = \frac{1}{2}\int_0^L \Big[I_0\left\{\left(\frac{\partial u}{\partial t}\right)^2 + \left(\frac{\partial w_b}{\partial t}\right)^2 + \left(\frac{\partial w_s}{\partial t}\right)^2 + 2\left(\frac{\partial w_b}{\partial t}\right)\left(\frac{\partial w_s}{\partial t}\right)\right\} - 2I_1\frac{\partial u}{\partial t}\frac{\partial^2 w_b}{\partial x \partial t} + I_2\left(\frac{\partial^2 w_b}{\partial x \partial t}\right)^2 + 2J_1\frac{\partial u}{\partial t}\frac{\partial^2 w_s}{\partial x \partial t} + 2J_2\left\{\left(\frac{\partial w_b}{\partial t}\right)\left(\frac{\partial w_z}{\partial t}\right) + \left(\frac{\partial w_s}{\partial t}\right)\left(\frac{\partial w_z}{\partial t}\right)\right\} - 2J_3\frac{\partial^2 w_b}{\partial x \partial t}\frac{\partial^2 w_s}{\partial x \partial t} + K_1\left(\frac{\partial^2 w_s}{\partial x \partial t}\right)^2 + K_2\left(\frac{\partial w_z}{\partial t}\right)^2\Big] dx \quad (13)$$

where t depicts time, and the associated inertial coefficients are provided by:

$$(I_0, I_1, I_2, J_1, J_2, J_3, K_1, K_2) = \int_{-\frac{h}{2}}^{+\frac{h}{2}} \rho\left(1, f_1, {f_1}^2, f_2, f_3, f_1 f_2, {f_2}^2, {f_3}^2\right) dz \quad (14)$$

To develop the FEM model using the variation formulation, Hermite-cubic polynomial function is employed to present displacement functions $u(x,t)$, $w_b(x,t)$, $w_s(x,t)$ and $w_z(x,t)$ as:

$$u(x,t) = \sum_{j=1}^{4} u_j \varphi_j(x) e^{i\omega t}, \tag{15a}$$

$$w_b(x,t) = \sum_{j=1}^{4} w_{b_j} \varphi_j(x) e^{i\omega t}, \tag{15b}$$

$$w_s(x,t) = \sum_{j=1}^{4} w_{s_j} \varphi_j(x) e^{i\omega t}, \tag{15c}$$

$$w_z(x,t) = \sum_{j=1}^{4} w_{z_j} \varphi_j(x) e^{i\omega t}, \tag{15d}$$

where ω is the natural frequency.

Nodal unknowns are revealed in the from of:

$$u_j = [u, u_{,x}] \tag{16a}$$

$$w_{b_j} = [w_b, w_{b,x}] \tag{16b}$$

$$w_{s_j} = [w_s, w_{s,x}] \tag{16c}$$

$$w_{z_j} = [w_z, w_{z,x}] \tag{16d}$$

By using the total energy (Π) of metal foam microbeams and Lagrange's equations, the governing equations are obtained as:

$$\Pi = U + V - K \tag{17}$$

$$\frac{\partial \Pi}{\partial q_j} - \frac{\partial}{\partial t}\left(\frac{\partial \Pi}{\partial \dot{q}_j}\right) = 0 \tag{18}$$

where q_j depicting the values of ($u_j, w_{b_j}, w_{s_j}, w_{z_j}$).

The developed FEM for flexural, elastic stability and free vibration problems are is revealed by:

$$\begin{bmatrix} [K_{11}] & [K_{12}] & [K_{13}] & [K_{14}] \\ [K_{12}]^T & [K_{22}] & [K_{23}] & [K_{24}] \\ [K_{13}]^T & [K_{23}]^T & [K_{33}] & [K_{34}] \\ [K_{14}]^T & [K_{24}]^T & [K_{34}]^T & [K_{44}] \end{bmatrix} \begin{Bmatrix} \{u_j\} \\ \{w_{b\,j}\} \\ \{w_{s\,j}\} \\ \{w_{z\,j}\} \end{Bmatrix} = \begin{Bmatrix} \{0\} \\ \{F_2\} \\ \{F_3\} \\ \{F_4\} \end{Bmatrix} \tag{19a}$$

$$\left(\begin{bmatrix} [K_{11}] & [K_{12}] & [K_{13}] & [K_{14}] \\ [K_{12}]^T & [K_{22}] & [K_{23}] & [K_{24}] \\ [K_{13}]^T & [K_{23}]^T & [K_{33}] & [K_{34}] \\ [K_{14}]^T & [K_{24}]^T & [K_{34}]^T & [K_{44}] \end{bmatrix} - N_0 \begin{bmatrix} [0] & [0] & [0] & [0] \\ [0]^T & [G_{22}] & [G_{23}] & [G_{24}] \\ [0]^T & [G_{23}]^T & [G_{33}] & [G_{34}] \\ [0]^T & [G_{24}]^T & [G_{34}]^T & [G_{44}] \end{bmatrix} \right) \begin{Bmatrix} \{u_j\} \\ \{w_{b\,j}\} \\ \{w_{s\,j}\} \\ \{w_{z\,j}\} \end{Bmatrix} = \begin{Bmatrix} \{0\} \\ \{0\} \\ \{0\} \\ \{0\} \end{Bmatrix} \tag{19b}$$

$$\left(\begin{bmatrix} [K_{11}] & [K_{12}] & [K_{13}] & [K_{14}] \\ [K_{12}]^T & [K_{22}] & [K_{23}] & [K_{24}] \\ [K_{13}]^T & [K_{23}]^T & [K_{33}] & [K_{34}] \\ [K_{14}]^T & [K_{24}]^T & [K_{34}]^T & [K_{44}] \end{bmatrix} - \omega^2 \begin{bmatrix} [M_{11}] & [M_{12}] & [M_{13}] & [0] \\ [M_{12}]^T & [M_{22}] & [M_{23}] & [M_{24}] \\ [M_{13}]^T & [M_{23}]^T & [M_{33}] & [M_{34}] \\ [M_{14}]^T & [M_{24}]^T & [M_{34}]^T & [M_{44}] \end{bmatrix} \right) \begin{Bmatrix} \{u_j\} \\ \{w_{b\,j}\} \\ \{w_{s\,j}\} \\ \{w_{z\,j}\} \end{Bmatrix} = \begin{Bmatrix} \{0\} \\ \{0\} \\ \{0\} \\ \{0\} \end{Bmatrix} \tag{19c}$$

where $[K_{kl}]$, $[M_{kl}]$, $[G_{kl}]$ matrices and F_k nodal force vector can be found in [50-53].

The kinematic boundary conditions can be provided by:

$Simply\ support\ (SS)$: $u = 0, w_b = 0, w_s = 0, w_z = 0\ at\ x = 0;\ w_b = 0, w_s = 0, w_z = 0\ at\ x = L$

$Clamped\ (CC)$: $u = w_b = w_{b,x} = \ w_s = w_{s,x} = w_z = w_{z,x} = 0\ at\ x = 0\ and\ x = L$

3. Numerical Examples

Metal foam microbeams with three different porosity distribution models, whose materials properties are $E_{max} = 200\ GPa$, $\nu = 0.3$, $\rho_{max} = 7800\ kg/m^3, \ell_{max} = 17.6\ \mu m$ [9], are analyzed. The effects of porosity distribution (UPD, NUPD1 and NUPD2), porosity parameters, Poisson's ratio, small size and boundary conditions (BC) on their displacements, frequencies and buckling loads are studied. Three MLSPs of MSGT are the same $(\ell = \ell_0 = \ell_1 = \ell_2)$ and two cases are considered:

constant value ($\ell = \ell_{max}$) and variable one ($\ell \neq \ell_{max}$). The necessary of including three MLSPs in the MSGT rather than only in the MCST and effects of variable MLSP on the responses of metal foam microbeams are discussed in details. For convenience, the dimensionless mid-span deflections (DMDs), fundamental frequencies (DFFs) and critical buckling loads (DCBLs) are normalized as $\overline{w} = w\frac{10^3 E_{max}h^3}{12qL^4}$, $\bar{\lambda} = \frac{\omega L^2}{h}\sqrt{\frac{\rho_{max}}{E_{max}}}$ and $\overline{N}_{cr} = N_0\frac{12L^2}{E_{max}h^3}$.

3.1 Verification studies

Since there are no available results for metal foam microbeams with various BCs using MSGT and NSDT. Thus, two verification studies are carried out: (a) metal foam macro-beams with various BCs using NSDT and (b) simply-support metal foam microbeams with MSGT and sinusoidal beam theory (SBT).

Tables 1-3 present the maximum deflections, fundamental frequencies and critical buckling loads of metal foams beams. The obtained results are compared with those by Fang et al. [13] and Chen et al. [5] who used NSDT and FSDT. It should be noted that the results with Poisson's effect given in Table 3 are obtained based on the constitutive relation $Q_{11} = \frac{E(z)(1-\nu)}{(1+\nu)(1-2\nu)}$ for NSDT and $Q_{11} = \frac{E(z)}{1-\nu^2}$ for TBT. The present results agree well with those using IGA and Ritz method. Some new results from TBT and NSDT are given as benchmark for future study in Tables 3 and 4.

To verify for metal foam microbeams with the size effect, Tables 5 and 6 show the comparison of deflections and natural frequencies predicted by the present approach and Wang et al. [42] using the SBT. For comparison purpose, the constitutive relation $Q_{11} = \frac{E(z)(1-\nu)}{(1+\nu)(1-2\nu)}$ for both NSDT and TBT in case of with Poisson's effect. An excellent agreement is found for all values of size effect (h/ℓ) and the porosity parameters (distribution and coefficients) confirming the validity of the present approach for the analysis of metal foam microbeams. Due to different theory, there is the

slightly variation in results of two models (TBT, SBT) and their results with NSDT, which includes the normal strain effect. Fig. 2 plots the results for three types of porosity distribution with respect to size effect (h/ℓ) and porosity coefficient (e_0). As e_0 increases and h/ℓ decreases, the DFFs/DCBLs decrease and DMDs increase. The greatest DMDs are for UPD distribution and the smallest one is for NUPD1 one. If one considers the inclusion of Poisson's effect, this leads to decrease displacements and increase buckling loads and frequencies. It should be noted that the results without Poisson's effect for microbeams agree better with those from experiments [55]. Thus, some new results without this effect for both MSGT and MCST are given in Tables 5-7 for the future reference. The corresponding ratios of the results of C-C metal foam microbeams versus h/ℓ are plotted in Fig. 3. Regardless of the porosity distribution, they are the same trend and nearly identical. At micron scale ($h/\ell = 1$), they are around 2.35, 1.55 and 0.42 for DCBL, DFF and DMD, respectively and gradually reach 1 as ($h/\ell = 20$). This confirms the importance of including three MLSPs in the MSGT rather than only in the MCST on the analysis of metal foam microbeams, especially at very small size $h/\ell \in [0, 20]$.

3.2 Parameter studies

In this section, effects of variable MLSP on the behaviours of metal foam microbeams are examined in details. It can be observed from Tables 8-10 that the results of variable MLSP ($\ell \neq \ell_{max}$) have smaller DMDs and higher DFFs/DCBLs than the constant one ($\ell = \ell_{max}$). In other words, the size-dependent of variable MLSP is stronger than constant one and depends on porosity distribution especially when $h/\ell = 1$. When the ratios of DFFs obtained for different h/ℓ ratios are examined, it can be determined that with the increase of the porosity parameter, they do not change in the analysis with a constant MLSP for UPD. However, it is observed that they decrease with the increase of the porosity parameter for NUPD1. This decrease becomes evident even with an increment in the aspect ratio. This observation is valid for all boundary conditions. Moreover, in the case of using variable

MLSP, it is found that the ratios of DFFs obtained at different h/ℓ ratios decrease in contrast for UPD with constant MSLP. Same observation is seen for the results produced by NUPD1. Based on the evaluations performed for the computational results of DMD and DCBL studies, it is revealed that all the statements explained above are also valid for these mechanical behaviours.

At this size, the ratios of DMD are approximately 2.1, 1.7 and 1.65 for UPD, NUPD2 and NUPD1 as revealed in Fig. 4. These ratios reach unity as h/ℓ increase. It can be seen in Fig. 4 that DMDs increase and DCBLs/DFFs decrease with the rise of porosity coefficient (e_0) and h/ℓ. This phenomenon can be explained by the increasing porosity coefficient leads to decrease both stiffness and density however, the reduction of the first one is more than second one. The variation of results among three porosity distributions is evident as e_0 increases. UPD metal foam microbeam has the largest DMDs and smallest DFFs/DCBLs. When the numerical results obtained for DMD, DCBL and DFF are examined, it is observed that the effect of variable MLSP is more dominant in the results of DMD and DCBL than those of DFF. With the increase in h/ℓ value, the ratio between the results of MSGT and MCST approaches 1, but numerical analysis associated with a strong size effect draws attention to the fact that there is a remarkable difference between the results produced by these two nonlocal theories. For the three metal foam microbeam models, first vibration mode shapes are depicted in Fig. 5. While there is axial mode is observed for constant MLSP ($\ell = \ell_{max}$), strong coupling between shear and bending components for variable one.

5. Conclusion

This paper investigates microbeams made of metal foams accompanied with various porosity models using the TBT and quasi-3D beam theories based on the MSGT. The governing equations are derived from Hamilton's principle and two nodes beam element is used to solve this problem. The present approach is validated by comparing the results with those available in the literature. Some important

effects related to small size, porosity coefficient, Poisson's ratio, variable MLSPs and end conditions on the behaviours of metal foam microbeams are discussed. Especially for very small scale ($h/\ell \in [0, 20]$), it is necessary to include three variable MLSPs in the MSGT for accuracy study of metal foam microbeams. Moreover, the effects of variable MLSP on structural responses of metal foam microbeams are significant for all cases in this paper. Especially, the ratios of DFFs obtained for different h/ℓ ratios are constant with the increasing of porosity parameter for UPD with constant MLSP. However, if one employs a variable MLSP for UPD, the ratio mentioned above changes with a change in the porosity parameter. Same statement can be provided for the results computed based on DMD and DCBL analysis. It is noteworthy that UPD metal foam microbeam has the largest DMDs and smallest DFFs/DCBLs for all cases. Some new results of these structures for both models (MCST, MSGT with constant and variable MLSP) and with/without Poison's effect can be used for future studies.

References

[1] Changdar A, Chakraborty S (2021) Laser processing of metal foam - A review. Journal of Manufacturing Processes 61:208-225. doi: 10.1016/j.jmapro.2020.10.012.

[2] Stasiewicz P, Magnucki K (2004) Elastic bending of an isotropic porous beam. International Journal of Applied Mechanics and Engineering 9:351–360.

[3] Stasiewicz P, Magnucki K (2004) Elastic buckling of a porous beam. Journal of Theoretical and Applied Mechanics 42:859–868.

[4] Magnucka-Blandzi E, Magnucki K (2007) Effective design of a sandwich beam with a metal foam core. Thin-Walled Structures 45:432-438. doi: 10.1016/j.tws.2007.03.005.

[5] Chen D, Yang J, Kitipornchai S (2015) Elastic buckling and static bending of shear deformable functionally graded porous beam. Composite Structures 133:54-61. doi: 10.1016/j.compstruct.2015.07.052

[6] Chen D, Yang J, Kitipornchai S (2016) Free and forced vibrations of shear deformable functionally graded porous beams. International Journal of Mechanical Sciences 108-109:14-22. doi: 10.1016/j.ijmecsci.2016.01.025

[7] Chen D, Kitipornchai S, Yang J (2016) Nonlinear free vibration of shear deformable sandwich beam with a functionally graded porous core. Thin-Walled Structures 107:39-48. doi: 10.1016/j.tws.2016.05.025

[8] Kitipornchai S, Chen D, Yang J (2017) Free vibration and elastic buckling of functionally graded porous beams reinforced by graphene platelets. Materials & Design 116:656-665. doi: 10.1016/j.matdes.2016.12.061

[9] Gao K, Huang Q, Kitipornchai S, Yang J (2019) Nonlinear dynamic buckling of functionally graded porous beams. Mechanics of Advanced Materials and Structures 28:418-429. doi: 10.1080/15376494.2019.1567888

[10] Lei Y, Gao K, Wang X, Yang J (2020) Dynamic behaviors of single- and multi-span functionally graded porous beams with flexible boundary constraints. Applied Mathematical Modelling 83:754-776. doi: 10.1016/j.apm.2020.03.017

[11] Gao K, Li R, Yang J (2019) Dynamic characteristics of functionally graded porous beams with interval material properties. Engineering Structures 197:109441. doi: 10.1016/j.engstruct.2019.109441

[12] Qin B, Zhong R, Wang Q, Zhao X (2020) A Jacobi-Ritz approach for FGP beams with arbitrary boundary conditions based on a higher-order shear deformation theory. Composite Structures 247:112435. doi: 10.1016/j.compstruct.2020.112435

[13] Fang W, Yu T, Van Lich L, Bui T (2019) Analysis of thick porous beams by a quasi-3D theory and isogeometric analysis. Composite Structures 221:110890. doi: 10.1016/j.compstruct.2019.04.062

[14] Wang Y, Zhao H (2019) Bending, buckling and vibration of shear deformable beams made of three-dimensional graphene foam material. Journal of the Brazilian Society of Mechanical Sciences and Engineering. doi: 10.1007/s40430-019-1926-1

[15] Hamed M, Abo-bakr R, Mohamed S, Eltaher M (2020) Influence of axial load function and optimization on static stability of sandwich functionally graded beams with porous core. Engineering with Computers 36:1929-1946. doi: 10.1007/s00366-020-01023-w

[16] Magnucki K, Malinowski M, Kasprzak J (2006) Bending and buckling of a rectangular porous plate. Steel and Composite Structures 6:319-333. doi: 10.12989/scs.2006.6.4.319

[17] Magnucka-Blandzi E (2011) Mathematical modelling of a rectangular sandwich plate with a metal foam core. Journal of Theoretical and Applied Mechanics 49:439–455.

[18] Ghorbanpour Arani A, Khani M, Khoddami Maraghi Z (2017) Dynamic analysis of a rectangular porous plate resting on an elastic foundation using high-order shear deformation theory. Journal of Vibration and Control 24:3698-3713. doi: 10.1177/1077546317709388

[19] Gao K, Gao W, Chen D, Yang J (2018) Nonlinear free vibration of functionally graded graphene platelets reinforced porous nanocomposite plates resting on elastic foundation. Composite Structures 204:831-846. doi: 10.1016/j.compstruct.2018.08.013

[20] Gao Z, Li H, Zhao J, Guan J, Wang Q (2021) Analyses of dynamic characteristics of functionally graded porous (FGP) sandwich plates with viscoelastic materials-filled square-celled core. Engineering Structures 248:113242. doi: 10.1016/j.engstruct.2021.113242

[21] Ebrahimi F, Dabbagh A, Taheri M (2020) Vibration analysis of porous metal foam plates rested on viscoelastic substrate. Engineering with Computers 37:3727-3739. doi: 10.1007/s00366-020-01031-w

[22] Chan D, Van Thanh N, Khoa N, Duc N (2020) Nonlinear dynamic analysis of piezoelectric functionally graded porous truncated conical panel in thermal environments. Thin-Walled Structures 154:106837. doi: 10.1016/j.tws.2020.106837

[23] Wang E, Li Q, Sun G (2020) Computational analysis and optimization of sandwich panels with homogeneous and graded foam cores for blast resistance. Thin-Walled Structures 147:106494. doi: 10.1016/j.tws.2019.106494

[24] Gao K, Gao W, Wu B, Wu D, Song C (2018) Nonlinear primary resonance of functionally graded porous cylindrical shells using the method of multiple scales. Thin-Walled Structures 125:281-293. doi: 10.1016/j.tws.2017.12.039

[25] Li H, Pang F, Ren Y, Miao X, Ye K (2019) Free vibration characteristics of functionally graded porous spherical shell with general boundary conditions by using first-order shear deformation theory. Thin-Walled Structures 144:106331. doi: 10.1016/j.tws.2019.106331

[26] Zhao J, Xie F, Wang A, Shuai C, Tang J, Wang Q (2019) A unified solution for the vibration analysis of functionally graded porous (FGP) shallow shells with general boundary conditions. Composites Part B: Engineering 156:406-424. doi: 10.1016/j.compositesb.2018.08.115

[27] Li H, Pang F, Chen H, Du Y (2019) Vibration analysis of functionally graded porous cylindrical shell with arbitrary boundary restraints by using a semi analytical method. Composites Part B: Engineering 164:249-264. doi: 10.1016/j.compositesb.2018.11.046

[28] Guan X, Sok K, Wang A, Shuai C, Tang J, Wang Q (2019) A general vibration analysis of functionally graded porous structure elements of revolution with general elastic restraints. Composite Structures 209:277-299. doi: 10.1016/j.compstruct.2018.10.103

[29] Foroutan K, Shaterzadeh A, Ahmadi H (2020) Nonlinear static and dynamic hygrothermal buckling analysis of imperfect functionally graded porous cylindrical shells. Applied Mathematical Modelling 77:539-553. doi: 10.1016/j.apm.2019.07.062

[30] Sajad Mirjavadi S, Forsat M, Barati M, Abdella G, Mohasel Afshari B, Hamouda A, Rabby S (2019) Dynamic response of metal foam FG porous cylindrical micro-shells due to moving loads with strain gradient size-dependency. The European Physical Journal Plus. doi: 10.1140/epjp/i2019-12540-3

[31] Toan Thang P, Nguyen-Thoi T, Lee J (2018) Mechanical stability of metal foam cylindrical shells with various porosity distributions. Mechanics of Advanced Materials and Structures 27:295-303. doi: 10.1080/15376494.2018.1472338

[32] Ebrahimi F, Seyfi A (2020) Studying propagation of wave in metal foam cylindrical shells with graded porosities resting on variable elastic substrate. Engineering with Computers. doi: 10.1007/s00366-020-01069-w

[33] Rostami R, Mohammadimehr M (2020) Vibration control of rotating sandwich cylindrical shell-reinforced nanocomposite face sheet and porous core integrated with functionally graded magneto-electro-elastic layers. Engineering with Computers. doi: 10.1007/s00366-020-01052-5

[34] Ebrahimi F, Habibi M, Safarpour H (2018) On modeling of wave propagation in a thermally affected GNP-reinforced imperfect nanocomposite shell. Engineering with Computers 35:1375-1389. doi: 10.1007/s00366-018-0669-4

[35] Wu H, Yang J, Kitipornchai S (2020) Mechanical Analysis of Functionally Graded Porous Structures: A Review. International Journal of Structural Stability and Dynamics 20:2041015. doi: 10.1142/s0219455420410151

[36] Yang F, Chong A, Lam D, Tong P (2002) Couple stress based strain gradient theory for elasticity, International Journal Of Solids And Structures. 39:2731-2743. doi:10.1016/s0020-7683(02)00152-x.

[37] Lam D, Yang F, Chong A, Wang J, Tong P (2003) Experiments and theory in strain gradient elasticity, Journal Of The Mechanics And Physics Of Solids. 51:1477-1508. doi:10.1016/s0022-5096(03)00053-x.

[38] Eringen A (1966) Linear theory of micropolar elasticity, Journal of Mathematics and Mechanics, 15(6):909-923.

[39] Lim CW, Zhang G, Reddy JN (2015). A higher-order nonlocal elasticity and strain gradient theory and its applications in wave propagation. Journal of the Mechanics and Physics of Solids, 78:298-313. doi: 10.1016/j.jmps.2015.02.001

[40] Wang Y, Liang C (2019) Wave propagation characteristics in nanoporous metal foam nanobeams. Results in Physics 12:287-297. doi: 10.1016/j.rinp.2018.11.080

[41] Amir S, Soleimani-Javid Z, Arshid E (2019) Size-dependent free vibration of sandwich micro beam with porous core subjected to thermal load based on SSDBT. ZAMM - Journal of Applied

Mathematics and Mechanics / Zeitschrift für Angewandte Mathematik und Mechanik. doi: 10.1002/zamm.201800334

[42] Wang Y, Zhao H, Ye C, Zu J (2018) A Porous Microbeam Model for Bending and Vibration Analysis Based on the Sinusoidal Beam Theory and Modified Strain Gradient Theory. International Journal of Applied Mechanics 10:1850059. doi: 10.1142/s175882511850059x

[43] Akbarzadeh Khorshidi M (2019) Effect of nano-porosity on postbuckling of non-uniform microbeams. SN Applied Sciences 1, 677. doi: 10.1007/s42452-019-0704-0

[44] Xie B, Sahmani S, Safaei B, Xu B (2020) Nonlinear secondary resonance of FG porous silicon nanobeams under periodic hard excitations based on surface elasticity theory. Engineering with Computers 37:1611-1634. doi: 10.1007/s00366-019-00931-w

[45] Phung-Van P, Ferreira A, Nguyen-Xuan H, Thai C (2021) A nonlocal strain gradient isogeometric nonlinear analysis of nanoporous metal foam plates. Engineering Analysis with Boundary Elements 130:58-68. doi: 10.1016/j.enganabound.2021.05.009

[46] Sahmani S, Fattahi A, Ahmed N (2019) Analytical treatment on the nonlocal strain gradient vibrational response of postbuckled functionally graded porous micro-/nanoplates reinforced with GPL. Engineering with Computers 36:1559-1578. doi: 10.1007/s00366-019-00782-5

[47] Arshid E, Khorasani M, Soleimani-Javid Z, Amir S, Tounsi A (2021) Porosity-dependent vibration analysis of FG microplates embedded by polymeric nanocomposite patches considering hygrothermal effect via an innovative plate theory. Engineering with Computers. doi: 10.1007/s00366-021-01382-y

[48] Sajad Mirjavadi S, Forsat M, Barati M, Abdella G, Mohasel Afshari B, Hamouda A, Rabby S (2019) Dynamic response of metal foam FG porous cylindrical micro-shells due to moving loads with strain gradient size-dependency. The European Physical Journal Plus. doi: 10.1140/epjp/i2019-12540-3

[49] Wang YQ, Liu YF & Zu JW (2019) On scale-dependent vibration of circular cylindrical nanoporous metal foam shells. Microsyst Technol 25, 2661–2674. doi: 10.1007/s00542-018-4262-y

[50] Karamanli A, Vo T (2021) Bending, vibration, buckling analysis of bi-directional FG porous microbeams with a variable material length scale parameter. Applied Mathematical Modelling 91:723-748. doi: 10.1016/j.apm.2020.09.058

[51] Karamanli A, Vo T (2021) A quasi-3D theory for functionally graded porous microbeams based on the modified strain gradient theory. Composite Structures 257:113066. doi: 10.1016/j.compstruct.2020.113066

[52] Karamanli A, Vo T (2020) Size-dependent behaviour of functionally graded sandwich microbeams based on the modified strain gradient theory. Composite Structures 246:112401. doi: 10.1016/j.compstruct.2020.112401

[53] Karamanli A, Vo T (2021) Finite element model for carbon nanotube-reinforced and graphene nanoplatelet-reinforced composite beams. Composite Structures 264:113739. doi: 10.1016/j.compstruct.2021.113739

[54] Karamanli A, Aydogdu M (2019) On the vibration of size dependent rotating laminated composite and sandwich microbeams via a transverse shear-normal deformation theory. Composite Structures 216:290-300. doi: 10.1016/j.compstruct.2019.02.044

[55] Dehrouyeh-Semnani A M, Nikkhah-Bahrami M (2015) A discussion on incorporating the Poisson effect in microbeam models based on modified couple stress theory Int J Eng Sci, 86 :20-25. doi: 10.1016/j.ijengsci.2014.10.003

[56] Ren H, Zhuang X, Oterkus E, Zhu H, Rabczuk T (2021) Nonlocal strong forms of thin plate, gradient elasticity, magneto-electro-elasticity and phase-field fracture by nonlocal operator method. Engineering with Computers. doi: 10.1007/s00366-021-01502-8

[57] Karami B, Janghorban M, Rabczuk T (2020) Dynamics of two-dimensional functionally graded tapered Timoshenko nanobeam in thermal environment using nonlocal strain gradient theory. Composites Part B: Engineering 182:107622. doi: 10.1016/j.compositesb.2019.107622

[58] Karami B, Janghorban M, Rabczuk T (2019) Analysis of elastic bulk waves in functionally graded triclinic nanoplates using a quasi-3D bi-Helmholtz nonlocal strain gradient model. European Journal of Mechanics - A/Solids 78:103822. doi: 10.1016/j.euromechsol.2019.103822

[59] Arefi M, Kiani M, Rabczuk T (2019) Application of nonlocal strain gradient theory to size dependent bending analysis of a sandwich porous nanoplate integrated with piezomagnetic face-sheets. Composites Part B: Engineering 168:320-333. doi: 10.1016/j.compositesb.2019.02.057

[60] Ma X, Sahmani S, Safaei B (2021) Quasi-3D large deflection nonlinear analysis of isogeometric FGM microplates with variable thickness via nonlocal stress–strain gradient elasticity. Engineering with Computers. doi: 10.1007/s00366-021-01390-y

[61] Chen S, Sahmani S, Safaei B (2021) Size-dependent nonlinear bending behavior of porous FGM quasi-3D microplates with a central cutout based on nonlocal strain gradient isogeometric finite element modelling. Engineering with Computers 37:1657-1678. doi: 10.1007/s00366-021-01303-z

[62] Thai C, Ferreira A, Nguyen-Xuan H, Nguyen L, Phung-Van P (2021) A nonlocal strain gradient analysis of laminated composites and sandwich nanoplates using meshfree approach. Engineering with Computers. doi: 10.1007/s00366-021-01501-9

[63] Moayedi H, Ebrahimi F, Habibi M, Safarpour H, Foong L (2020) Application of nonlocal strain–stress gradient theory and GDQEM for thermo-vibration responses of a laminated composite nanoshell. Engineering with Computers 37:3359-3374. doi: 10.1007/s00366-020-01002-1

[64] Thang P, Do D, Lee J, Nguyen-Thoi T (2021) Size-dependent analysis of functionally graded carbon nanotube-reinforced composite nanoshells with double curvature based on nonlocal strain gradient theory. Engineering with Computers. doi: 10.1007/s00366-021-01517-1

[65] Thai T, Rabczuk T, Bazilevs Y, Meschke G (2016) A higher-order stress-based gradient-enhanced damage model based on isogeometric analysis. Computer Methods in Applied Mechanics and Engineering 304:584-604. doi: 10.1016/j.cma.2016.02.031

[66] Bisheh H, Wu N, Rabczuk T (2021) A study on the effect of electric potential on vibration of smart nanocomposite cylindrical shells with closed circuit. Thin-Walled Structures 166:108040. doi: 10.1016/j.tws.2021.108040

[67] Arefi M, Mohammad-Rezaei Bidgoli E, Rabczuk T (2019) Effect of various characteristics of graphene nanoplatelets on thermal buckling behavior of FGRC micro plate based on MCST. European Journal of Mechanics - A/Solids 77:103802. doi: 10.1016/j.euromechsol.2019.103802

[68] Aria A, Rabczuk T, Friswell M (2019) A finite element model for the thermo-elastic analysis of functionally graded porous nanobeams. European Journal of Mechanics - A/Solids 77:103767. doi: 10.1016/j.euromechsol.2019.04.002

[69] Sahmani S, Aghdam M, Rabczuk T (2018) Nonlocal strain gradient plate model for nonlinear large-amplitude vibrations of functionally graded porous micro/nano-plates reinforced with GPLs. Composite Structures 198:51-62. doi: 10.1016/j.compstruct.2018.05.031

[70] Thai T, Zhuang X, Rabczuk T (2021) A nonlinear geometric couple stress based strain gradient Kirchhoff–Love shell formulation for microscale thin-wall structures. International Journal of Mechanical Sciences 196:106272. doi: 10.1016/j.ijmecsci.2021.106272

[71] Adab N, Arefi M, Amabili M (2022) A comprehensive vibration analysis of rotating truncated sandwich conical microshells including porous core and GPL-reinforced face-sheets. Composite Structures 279:114761. doi: 10.1016/j.compstruct.2021.114761

[72] Dehsaraji M, Arefi M, Loghman A (2021) Size dependent free vibration analysis of functionally graded piezoelectric micro/nano shell based on modified couple stress theory with considering thickness stretching effect. Defence Technology 17:119-134. doi: 10.1016/j.dt.2020.01.001

[73] Dehsaraji M, Arefi M, Loghman A (2020) Three dimensional free vibration analysis of functionally graded nano cylindrical shell considering thickness stretching effect. Steel and Composite Structures 34(5):657-670. doi.org/10.12989/scs.2020.34.5.657

[74] Arefi M, Amabili M (2021) A comprehensive electro-magneto-elastic buckling and bending analyses of three-layered doubly curved nanoshell, based on nonlocal three-dimensional theory. Composite Structures 257:113100. doi: 10.1016/j.compstruct.2020.113100

Table 1: Comparison the maximum displacements of metal foam beams under uniform load with various L/h and BCs (e_0 = 0.5).

BCs	Porosity distribution	Reference	L/h =5	10	20	40
CF	UPD	Fang et al. [13] (Q3D)	0.00007	0.00114	0.01813	0.28976
		Present (Q3D)	0.00007	0.00114	0.01811	0.28934
	NUPD1	Fang et al. [13] (Q3D)	0.00006	0.00092	0.01466	0.23422
		Present (Q3D)	0.00006	0.00092	0.01465	0.23384
	NUPD2	Fang et al. [13] (Q3D)	0.00007	0.00111	0.01765	0.28216
		Present (Q3D)	0.00007	0.00111	0.01764	0.28176
CC	UPD	Present (Q3D)	0.000002	0.00003	0.00039	0.00605
	NUPD1	Present (Q3D)	0.000002	0.00002	0.00032	0.00490
	NUPD2	Present (Q3D)	0.000002	0.00003	0.00038	0.00589
CS	UPD	Present (Q3D)	0.000004	0.00005	0.00079	0.01257
	NUPD1	Present (Q3D)	0.000003	0.00004	0.00064	0.01017
	NUPD2	Present (Q3D)	0.000004	0.00005	0.00077	0.01217
SS	UPD	Present (Q3D)	0.000008	0.00012	0.00190	0.03026
	NUPD1	Present (Q3D)	0.000007	0.00010	0.00154	0.02447
	NUPD2	Present (Q3D)	0.000008	0.00012	0.00185	0.02947

Table 2: Comparison the natural frequencies for metal foam beams with various BCs (L/h = 10, e_0= 0.5)

BCs	Porosity distribution	Reference	Natural frequencies		
			Mode 1	Mode 2	Mode 3
CF	UPD	Fang et al. [13] (Q3D)	0.0859	0.5152	1.3564
		Present (Q3D)	0.0859	0.5152	1.3565
	NUPD1	Fang et al. [13] (Q3D)	0.0875	0.5649	1.3794
		Present (Q3D)	0.0953	0.5649	1.4379
	NUPD2	Fang et al. [13] (Q3D)	0.0870	0.5216	1.3717
		Present (Q3D)	0.0870	0.5215	1.3711
CC	UPD	Fang et al. [13] (Q3D)	0.51848	1.3516	2.4087
		Present (Q3D)	0.5186	1.3518	2.4102
	NUPD1	Fang et al. [13] (Q3D)	0.5653	1.4541	2.5424
		Present (Q3D)	0.5654	1.4543	2.5441
	NUPD2	Fang et al. [13] (Q3D)	0.5248	1.3669	2.4334
		Present (Q3D)	0.5248	1.3667	2.4339
CS	UPD	Fang et al. [13] (Q3D)	0.3672	1.1218	1.4168
		Present (Q3D)	0.3673	1.1218	2.1739
	NUPD1	Fang et al. [13] (Q3D)	0.4043	1.2159	1.4379
		Present (Q3D)	0.4043	1.2160	2.3192
	NUPD2	Fang et al. [13] (Q3D)	0.3719	1.1350	1.4342
		Present (Q3D)	0.3729	1.1352	2.1946
SS	UPD	Present (Q3D)	0.2384	0.9114	1.4168
	NUPD1	Present (Q3D)	0.2639	0.9969	1.4379
	NUPD2	Present (Q3D)	0.2414	0.9209	1.4294

Table 3: Comparison the critical buckling loads of metal foam beams with different BCs (e_0= 0.5) ($P_{cr} = \frac{N_{x0}}{A_{110}}$; $A_{110} = \frac{0.5E_1h}{1-v^2}$)

BCs	Porosity distribution	Reference	With Poisson's effect			Without Poisson's effect		
			L/h =5	10	20	L/h =5	10	20
CF	UPD	Present (TBT)	0.01057	0.00270	0.0006792	0.00943	0.00240	0.0006038
		Present (Q3D)	0.01076	0.00272	0.0006825	0.00952	0.00241	0.0006052
	NUPD1	Chen et al. [5] (FBT)	-	0.00334	0.0008402	-	-	-
		Present (TBT)	0.01295	0.00333	0.0008400	0.01563	0.00297	0.0007469
		Present (Q3D)	0.01317	0.00336	0.0008440	0.01167	0.00298	0.0007485
	NUPD2	Chen et al. [5] (FBT)	-	0.00276	0.0006939	-	-	-
		Present (TBT)	0.01080	0.00276	0.0006934	0.00963	0.00246	0.0006169
		Present (Q3D)	0.01111	0.00281	0.0007054	0.00977	0.00248	0.0006215
CC	UPD	Present (TBT)	0.11841	0.03894	0.0105739	0.10912	0.03503	0.0094292
		Present (Q3D)	0.12321	0.03993	0.0107076	0.11169	0.03551	0.0094887
	NUPD1	Chen et al. [5] (FBT)	-	-	0.0130109	-	-	-
		Present (TBT)	0.13151	0.04643	0.0129526	0.12215	0.04192	0.0115632
		Present (Q3D)	0.13508	0.04747	0.0131092	0.12408	0.04243	0.0116328
	NUPD2	Chen et al. [5] (FBT)	-	-	0.0108060	-	-	-
		Present (TBT)	0.12050	0.03973	0.0107997	0.11108	0.03574	0.0096308
		Present (Q3D)	0.12599	0.04112	0.0110561	0.11391	0.03638	0.0097380
CS	UPD	Present (TBT)	0.07175	0.02100	0.0054849	0.06519	0.01876	0.0048836
		Present (Q3D)	0.07382	0.02129	0.0055200	0.06630	0.01893	0.0048993
	NUPD1	Chen et al. [5] (FBT)	-	-	0.0067559	-	-	-
		Present (TBT)	0.08302	0.02547	0.0067520	0.07588	0.02283	0.0060153
		Present (Q3D)	0.08487	0.02579	0.0067936	0.07688	0.02299	0.0060339
	NUPD2	Chen et al. [5] (FBT)	-	-	0.0056383	-	-	-
		Present (TBT)	0.07357	0.02159	0.0056446	0.06686	0.01932	0.0050259
		Present (Q3D)	0.07614	0.02208	0.0057345	0.06817	0.01954	0.0050630
SS	UPD	Present (TBT)	0.03894	0.01057	0.0027017	0.03503	0.00943	0.0024053
		Present (Q3D)	0.03937	0.01061	0.0027042	0.03530	0.00945	0.0024050
	NUPD1	Chen et al. [5] (FBT)	-	-	0.0033387	-	-	-
		Present (TBT)	0.04643	0.01295	0.0033349	0.04198	0.01156	0.0029763
		Present (Q3D)	0.04686	0.01299	0.0033378	0.04219	0.01159	0.0029693
	NUPD2	Chen et al. [5] (FBT)	-	-	0.0028688	-	-	-
		Present (TBT)	0.03973	0.01080	0.0027601	0.03574	0.00963	0.0024555
		Present (Q3D)	0.04058	0.01096	0.0027951	0.03617	0.00970	0.0024697

Table 4: DFFs and DMDs of metal foam beams with different BCs (e_0= 0.5).

BCs	Porosity distribution	Reference	DFFs			DMD		
			L/h =5	10	20	L/h =5	10	20
CF	UPD	Present (TBT)	0.8877	0.9082	0.9136	19.6743	19.0856	18.9366
		Present (Q3D)	0.8934	0.9112	0.9155	19.5032	18.9821	18.8659
	NUPD1	Present (TBT)	0.9790	1.0080	1.0158	16.1231	15.4788	15.3154
		Present (Q3D)	0.9852	1.0112	1.0178	15.9839	15.3968	15.2590
	NUPD2	Present (TBT)	0.8968	0.9179	0.9235	19.2654	18.6823	18.5347
		Present (Q3D)	0.9046	0.9231	0.9277	19.0091	18.4897	18.3725
CC	UPD	Present (TBT)	4.6994	5.4597	5.7260	0.5857	0.4426	0.4059
		Present (Q3D)	4.7612	5.5001	5.7502	0.5723	0.4369	0.4027
	NUPD1	Present (TBT)	4.9476	5.9530	6.3338	0.5278	0.3717	0.3315
		Present (Q3D)	5.0098	5.9966	6.3604	0.5164	0.3670	0.3290
	NUPD2	Present (TBT)	4.7395	5.5140	5.7864	0.5754	0.4338	0.3974
		Present (Q3D)	4.8083	5.5662	5.8246	0.5608	0.4264	0.3924
CS	UPD	Present (TBT)	3.5547	3.8801	3.9793	1.0111	0.8670	0.8305
		Present (Q3D)	3.5839	3.8954	3.9880	0.9932	0.8600	0.8269
	NUPD1	Present (TBT)	3.8246	4.2714	4.4145	0.8724	0.7146	0.6746
		Present (Q3D)	3.8558	4.2884	4.4241	0.8578	0.7090	0.6717
	NUPD2	Present (TBT)	3.5871	3.9199	4.0217	0.9919	0.8491	0.8130
		Present (Q3D)	3.6236	3.9446	4.0405	0.9710	0.8385	0.8055
SS	UPD	Present (TBT)	2.4121	2.5268	2.5588	2.1686	2.0177	1.9799
		Present (Q3D)	2.4167	2.5281	2.5591	2.1491	2.0129	1.9788
	NUPD1	Present (TBT)	2.6379	2.7973	2.8430	1.8106	1.6449	1.6035
		Present (Q3D)	2.6434	2.7990	2.8434	1.7956	1.6413	1.6026
	NUPD2	Present (TBT)	2.4319	2.5523	2.5860	2.1250	1.9754	1.9380
		Present (Q3D)	2.4432	2.5604	2.5931	2.9070	1.9610	1.9269

Table 5. Comparison the displacements of S-S metal foam microbeams under uniform load for various h/ℓ $(e_0 = 0.5, L/h = 10)$

Porosity distribution	Reference	Theory	Poisson's effect	h/ℓ $(e_0 = 0.5)$			e_0 $(h/\ell = 1)$		
				$h/\ell = 1$	4	8	0.1	0.4	0.8
UPD	Wang et al. [42] (SBT, $\varepsilon_z = 0$)	MSGT	x	1.1556	8.1887	11.7705	0.8174	1.0426	1.8209
	Present (TBT, $\varepsilon_z = 0$)	MSGT	x	1.1717	8.2326	11.7883	0.8288	1.0571	1.8463
			-	1.2034	10.1377	16.1618	0.8512	1.0857	1.8963
		MCST	x	3.3278	11.5119	13.1330	2.3538	3.0023	5.2438
			-	3.6088	15.6761	18.8248	2.5525	3.2558	5.6866
	Present ($\varepsilon_z \neq 0$)	MSGT	x	1.5577	10.8133	15.4110	1.1018	1.4054	2.4546
			-	1.5660	11.4029	16.8476	1.1076	1.4128	2.4677
		MCST	x	3.5481	14.3302	16.8976	2.5096	3.2010	5.5910
			-	3.6191	15.6631	18.7895	2.5598	3.2652	5.7029
NUPD1	Wang et al. [42] (SBT, $\varepsilon_z = 0$)	MSGT	x	1.0925	7.1132	9.8378	0.8135	1.0061	1.4743
	Present (TBT, $\varepsilon_z = 0$)	MSGT	x	1.1074	7.1532	9.8512	0.8248	1.0198	1.4946
			-	1.1432	8.9510	13.5942	0.8477	1.0514	1.5526
		MCST	x	3.0736	9.6401	10.8184	2.3348	2.8482	4.0305
			-	3.3753	13.2266	15.5028	2.5368	3.1176	4.4889
	Present ($\varepsilon_z \neq 0$)	MSGT	x	1.4741	9.3808	12.8476	1.0967	1.3571	1.9920
			-	1.4835	9.9431	14.0816	1.1027	1.3654	2.0074
		MCST	x	3.3107	12.0711	13.9192	2.4932	3.0599	4.3907
			-	3.3874	13.2240	15.4783	2.5443	3.1282	4.5081
NUPD2	Wang et al. [42] (SBT, $\varepsilon_z = 0$)	MSGT	x	1.1207	7.9842	11.5082	0.8162	1.0244	1.5743
	Present (TBT, $\varepsilon_z = 0$)	MSGT	x	1.1354	8.0254	11.5248	0.8276	1.0382	1.5907
			-	1.1659	9.8755	15.7925	0.8501	1.0664	1.6278
		MCST	x	3.2351	11.2527	12.8532	2.3493	2.9510	4.6500
			-	3.5068	15.3154	18.4188	2.5484	3.2011	4.9945
	Present ($\varepsilon_z \neq 0$)	MSGT	x	1.5082	10.4649	14.9194	1.1003	1.3797	2.1045
			-	1.5164	11.0621	16.3846	1.1061	1.3871	2.1157
		MCST	x	3.4408	13.8823	16.3656	2.5053	3.1435	4.8741
			-	3.5137	15.2458	18.3012	2.5558	3.2088	4.9878

Table 6. Comparison the fundamental frequencies of S-S metal foam microbeams for various $h/\ell, e_0 (L/h = 10)$.

Porosity distribution	Reference	Theory	Poisson's effect	h/ℓ ($e_0 = 0.5$)			e_0 ($h/\ell = 1$)		
				$h/\ell = 1$	4	8	0.1	0.4	0.8
UPD	Wang et al. [42] (SBT, $\varepsilon_z = 0$)	MSGT	x	36.5809	13.7403	11.4598	39.8889	37.5344	32.6498
	Present (TBT, $\varepsilon_z = 0$)	MSGT	x	36.3244	13.7029	11.4510	39.6093	37.2712	32.4209
			-	35.8432	12.3489	9.7802	39.0846	36.7775	31.9914
		MCST	x	21.5565	11.5882	10.8489	23.5059	22.1184	19.2400
			-	20.7005	9.9310	9.0621	22.5725	21.2401	18.4760
	Present ($\varepsilon_z \neq 0$)	MSGT	x	31.4697	11.9448	10.0057	34.3155	32.2900	28.0879
			-	31.3871	11.6340	9.5723	34.2255	32.2053	28.0142
		MCST	x	20.8538	10.3765	9.5556	22.7397	21.3974	18.6128
			-	20.6543	9.9285	9.0647	22.5221	21.1926	18.4347
NUPD1	Wang et al. [42] (SBT, $\varepsilon_z = 0$)	MSGT	x	37.6097	14.7371	12.5299	39.9812	38.2000	36.2565
	Present (TBT, $\varepsilon_z = 0$)	MSGT	x	37.3519	14.6950	12.5212	39.7027	27.9378	36.0045
			-	36.7617	13.1372	10.6596	39.1618	37.3641	35.3264
		MCST	x	22.4217	12.6581	11.9482	23.5998	22.7024	21.9257
			-	21.3962	10.8072	9.9818	22.6412	21.6996	20.7761
	Present ($\varepsilon_z \neq 0$)	MSGT	x	32.3460	12.8222	10.9563	34.3940	32.8567	31.1692
			-	32.2435	12.4563	10.4676	34.3010	32.7573	31.0495
		MCST	x	21.5845	11.3035	10.5260	22.8135	21.8825	20.9942
			-	21.3440	10.8024	9.9845	22.5898	21.6477	20.7222
NUPD2	Wang et al. [42] (SBT, $\varepsilon_z = 0$)	MSGT	x	37.1428	13.9141	11.5888	39.9161	37.8641	35.1080
	Present (TBT, $\varepsilon_z = 0$)	MSGT	x	36.8730	13.8712	11.5750	39.6364	37.5941	34.8067
			-	36.3786	12.5049	9.8854	39.1087	37.0890	34.3696
		MCST	x	21.8500	11.7145	10.9605	23.5279	22.3024	20.3755
			-	20.9859	10.0417	9.1564	22.5900	21.4131	19.6573
	Present ($\varepsilon_z \neq 0$)	MSGT	x	31.9719	12.1389	10.1666	34.3392	32.5838	30.2890
			-	31.8813	11.8075	9.7029	34.2485	32.4939	30.1876
		MCST	x	21.1707	10.5399	9.7071	22.7587	21.5892	19.9067
			-	20.9527	10.0595	9.1812	22.5397	21.3727	19.6706

Table 7. The critical buckling loads of S-S metal foam microbeams under point and uniform load for various $h/\ell, e_0 (L/h = 10)$

Porosity distribution	Reference	Theory	Poisson's effect	h/ℓ ($e_0 = 0.5$)			e_0 ($h/\ell = 1$)		
				$h/\ell = 1$	4	8	e_0=0.1	0.4	0.8
UPD	Present (TBT, $\varepsilon_z = 0$)	MSGT	x	109.5788	15.5951	10.8908	154.9247	121.4588	69.5400
			-	106.6972	12.6670	7.9459	150.8506	118.2648	67.7113
		MCST	x	38.6030	11.1538	9.7758	54.5777	42.7881	24.4979
			-	35.6000	8.1931	6.8221	50.3320	39.4596	22.5922
	Present ($\varepsilon_z \neq 0$)	MSGT	x	82.4275	11.8744	8.3319	116.5376	91.3639	52.3095
			-	81.9930	11.2613	7.6222	115.9233	90.8823	52.0337
		MCST	x	36.1978	8.9607	7.5988	51.1771	40.1221	22.9715
			-	35.4913	8.1992	6.8346	50.1783	39.3391	22.5232
NUPD1	Present (TBT, $\varepsilon_z = 0$)	MSGT	x	115.0899	17.9469	13.0292	155.6770	125.9239	85.9403
			-	112.3358	14.3459	9.4452	151.4676	122.1469	82.7361
		MCST	x	41.7973	13.3164	11.8637	55.0211	45.1037	31.8749
			-	38.0637	9.7089	8.2822	50.6447	41.2096	28.6221
	Present ($\varepsilon_z \neq 0$)	MSGT	x	87.1265	13.6866	9.9917	117.0802	94.6343	64.4894
			-	86.5721	12.9138	9.1175	116.4443	94.0597	63.9936
		MCST	x	38.7939	10.6350	9.2219	51.5129	41.9739	29.2521
			-	37.9204	9.7095	8.2945	50.4844	41.0618	28.4938
NUPD2	Present (TBT, $\varepsilon_z = 0$)	MSGT	x	113.0899	15.9980	11.1398	155.1459	123.6800	80.7273
			-	110.1305	13.0036	8.1317	151.0465	120.4109	78.8882
		MCST	x	39.7099	11.4106	9.9885	54.6823	43.5329	27.6281
			-	36.6358	8.3861	6.9725	50.4123	40.1342	25.7243
	Present ($\varepsilon_z \neq 0$)	MSGT	x	85.1384	12.2700	8.6062	116.7020	93.0704	61.0199
			-	84.6786	11.6084	7.8375	116.0832	92.5693	60.6980
		MCST	x	37.3278	9.2497	7.8457	51.2641	40.8577	26.3531
			-	36.5569	8.4236	7.0168	50.2584	40.0301	25.7550

Table 8. DFFs of the metal foam microbeams for various $e_0, L/h, h/\ell$ and BCs

L/h	Porosity distribution	h/ℓ	S-S			C-F			C-C		
			e_0 =0.1	0.5	0.8	0.1	0.5	0.8	0.1	0.5	0.8
MSGT ($\ell = \ell_{max}$)											
5	UPD	1	8.4140	7.7162	6.8870	3.6040	3.3051	2.9500	19.1581	17.5693	15.6813
		2	5.2613	4.8250	4.3065	1.9965	1.8310	1.6342	11.0139	10.1005	9.0151
		8	2.8802	2.6414	2.3575	1.0709	0.9821	0.8766	5.7833	5.3037	4.7338
	NUPD1	1	8.4167	7.8310	7.4440	3.6139	3.4062	3.2883	19.1644	17.8308	16.9496
		2	5.2892	5.0594	4.9856	2.0058	1.9120	1.8761	11.0993	10.7567	10.7669
		8	2.9117	2.8636	2.8988	1.0834	1.0708	1.0933	5.8264	5.6088	5.4819
20	UPD	1	10.0118	9.1815	8.1948	3.6126	3.3130	2.9569	22.8645	20.9683	18.7150
		2	5.5824	5.1194	4.5693	2.0102	1.8435	1.6454	12.7062	11.6525	10.4003
		8	3.0501	2.7971	2.4965	1.0924	1.0018	0.8942	6.8748	6.3047	5.6272
	NUPD1	1	10.0288	9.4041	9.0344	3.6186	3.3929	3.2595	22.9203	21.5715	20.8013
		2	5.6058	5.3319	5.2215	2.0186	1.9196	1.8794	12.7642	12.1626	11.9339
		8	3.0880	3.0666	3.1577	1.1061	1.0988	1.1321	6.9575	6.8907	7.0612
MSGT ($\ell \neq \ell_{max}$)											
5	UPD	1	8.3930	6.0175	3.8084	3.3906	2.2919	1.4412	18.7923	12.6761	7.9338
		2	5.0133	3.6843	2.6779	1.9005	1.3886	1.0017	10.4763	7.6180	5.4540
		8	2.8512	2.5186	2.1945	1.0595	0.9339	0.8124	5.7168	5.0187	4.3503
	NUPD1	1	8.3964	6.9632	6.2456	3.4173	2.6216	2.3409	18.8500	15.7229	14.4389
		2	5.0679	4.2013	3.9696	1.9173	1.5732	1.4802	10.6963	9.1136	8.6797
		8	2.8857	2.7742	2.7962	1.0730	1.0352	1.0536	5.7766	5.4235	5.2325
20	UPD	1	9.4227	6.3870	4.0396	3.3996	2.3023	1.4536	21.5149	14.5624	9.1830
		2	5.3187	3.9065	2.8374	1.9147	1.4041	1.0178	12.1004	8.8633	6.4146
		8	3.0192	2.6665	2.3233	1.0813	0.9545	0.8313	6.8034	6.0016	5.2243
	NUPD1	1	9.4630	7.1879	6.4034	3.4141	2.5922	2.3088	21.6573	16.5624	14.7871
		2	5.3531	4.3794	4.1262	1.9271	1.5746	1.4825	12.1975	10.0051	9.4267
		8	3.0587	2.9669	3.0504	1.0955	1.0626	1.0933	6.8913	6.6643	6.8116

Table 9. DCBLs of the metal foam microbeams for various $e_0, L/h, h/\ell$ and BCs

L/h	Porosity distribution	h/ℓ	S-S			C-F			C-C		
			e_0 =0.1	0.5	0.8	0.1	0.5	0.8	0.1	0.5	0.8
MSGT ($\ell = \ell_{max}$)											
5	UPD	1	107.8373	76.2738	48.4042	30.1038	21.2925	13.5125	366.7850	259.4285	164.6364
		2	33.5771	23.7492	15.0715	9.2964	6.5754	4.1728	112.4131	79.5103	50.4582
		8	10.0603	7.1157	4.5157	2.7251	1.9275	1.2232	32.2435	22.8060	14.4729
	NUPD1	1	108.7205	82.3297	62.0275	30.2497	22.5304	16.6875	372.8811	295.2095	234.3500
		2	33.9436	26.1653	20.2949	9.3808	7.1611	5.4907	114.1473	90.1331	71.9865
		8	10.2807	8.3596	6.8163	2.7914	2.3043	1.9301	32.7162	25.4589	19.3438
20	UPD	1	118.1943	83.5993	53.0531	30.0011	21.2199	13.4664	474.2265	335.4223	212.8630
		2	36.7443	25.9894	16.4932	9.3068	6.5827	4.1775	146.9083	103.9089	65.9418
		8	10.9677	7.7575	4.9230	2.7628	1.9541	1.2401	43.4085	30.7030	19.4845
	NUPD1	1	118.5980	87.7100	64.4961	30.0980	22.2401	16.3415	476.4162	354.4231	262.1758
		2	37.0542	28.1947	21.5426	9.3842	7.1360	5.4482	148.2327	113.1244	86.7138
		8	11.2425	9.3251	7.8780	2.8324	2.3516	1.9904	44.4663	36.7226	30.7818
MSGT ($\ell \neq \ell_{max}$)											
5	UPD	1	95.5302	36.9380	11.7866	26.6548	10.2697	3.2532	324.6126	124.6600	39.2254
		2	30.4864	13.8477	5.8274	8.4310	3.8046	1.5881	101.8412	45.6766	18.9137
		8	9.8586	6.4690	3.9125	2.6691	1.7480	1.0558	31.5620	20.6197	12.4303
	NUPD1	1	97.7536	49.7706	32.0255	27.0048	13.2744	8.4255	341.0745	192.3514	129.9320
		2	31.1783	18.0759	12.8853	8.5649	4.8417	3.4218	106.1242	65.0071	47.0004
		8	10.0985	7.8467	6.3407	2.7384	2.1553	1.7967	32.1902	23.9169	17.7531
20	UPD	1	104.6949	40.4539	12.8910	26.5711	10.2575	3.2625	419.9742	162.0304	51.4707
		2	33.3550	15.1327	6.3593	8.4458	3.8253	1.6042	133.2915	60.2998	25.2462
		8	10.7470	7.0500	4.2635	2.7068	1.7749	1.0730	42.5226	27.8614	16.8337
	NUPD1	1	105.5947	51.2424	32.4004	26.7859	12.9735	8.1973	425.1576	208.6001	132.3565
		2	33.7881	19.0208	13.4524	8.5526	4.8039	3.3942	135.3488	76.5664	54.1745
		8	11.0298	8.7287	7.3518	2.7784	2.2002	1.8570	43.6277	34.3673	28.6750

Table 10. DMDs of the metal foam microbeams for various $e_0, L/h, h/\ell$ and BCs

L/h	Porosity distribution	h/ℓ	S-S			C-F			C-C		
			e_0 =0.1	0.5	0.8	0.1	0.5	0.8	0.1	0.5	0.8
MSGT ($\ell = \ell_{max}$)											
5	UPD	1	1.1859	1.6767	2.6421	10.1018	14.2822	22.5054	0.2745	0.3881	0.6115
		2	3.8097	5.3862	8.4875	32.8993	46.5136	73.2946	0.9021	1.2754	2.0097
		8	12.7228	17.9878	28.3445	114.1889	161.4425	254.3956	3.2599	4.6089	7.2625
	NUPD1	1	1.1765	1.5550	2.0661	10.0467	13.4458	18.0925	0.2700	0.3409	0.4295
		2	3.7689	4.8915	6.3098	32.5919	42.6196	55.4859	0.8881	1.1231	1.4047
		8	12.4484	15.2963	18.7330	111.5177	135.3998	162.3473	3.2115	4.1193	5.4118
20	UPD	1	1.0871	1.5370	2.4219	10.1911	14.4084	22.7043	0.2142	0.3029	0.4773
		2	3.4968	4.9439	7.7904	32.9122	46.5319	73.3234	0.6937	0.9808	1.5455
		8	11.7152	16.5632	26.0998	111.4272	157.5379	248.2429	2.3692	3.3497	5.2783
	NUPD1	1	1.0834	1.4650	1.9924	10.1572	13.7379	18.6848	0.2132	0.2863	0.3865
		2	3.4676	4.5573	5.9648	32.6394	42.9139	56.1974	0.6874	0.9003	1.1738
		8	11.4288	13.7783	16.3079	108.6918	130.9454	154.7796	2.3131	2.8031	3.3488
MSGT ($\ell \neq \ell_{max}$)											
5	UPD	1	1.3387	3.4626	10.8539	11.4129	29.6946	94.2206	0.3103	0.8103	2.5934
		2	4.1961	9.2396	21.9608	36.3055	80.8346	194.8835	0.9969	2.2390	5.4752
		8	12.9833	19.7872	32.7171	116.6466	178.5149	296.0970	3.3361	5.1471	8.6014
	NUPD1	1	1.3090	2.5764	4.0082	11.2417	22.7337	35.7340	0.2952	0.5238	0.7757
		2	4.1043	7.0881	9.9468	35.6814	63.0051	89.1607	0.9557	1.5607	2.1557
		8	12.6737	16.2981	20.1359	113.6879	144.8745	174.7686	3.2669	4.4041	5.9358
20	UPD	1	1.2273	3.1762	9.9673	11.5080	29.8341	93.9522	0.2420	0.6280	1.9823
		2	3.8522	8.4908	20.2051	36.2765	80.2109	191.6185	0.7649	1.6950	4.0621
		8	11.9558	18.2255	30.1373	113.7442	173.5607	287.1952	2.4193	3.6965	6.1237
	NUPD1	1	1.2168	2.5078	3.9663	11.4113	23.5392	37.2453	0.2388	0.4858	0.7649
		2	3.8029	6.7557	9.5522	35.8146	63.7809	90.3090	0.7528	1.3306	1.8813
		8	11.6493	14.7197	17.4751	110.8127	139.9998	165.9662	2.3578	2.9967	3.5985

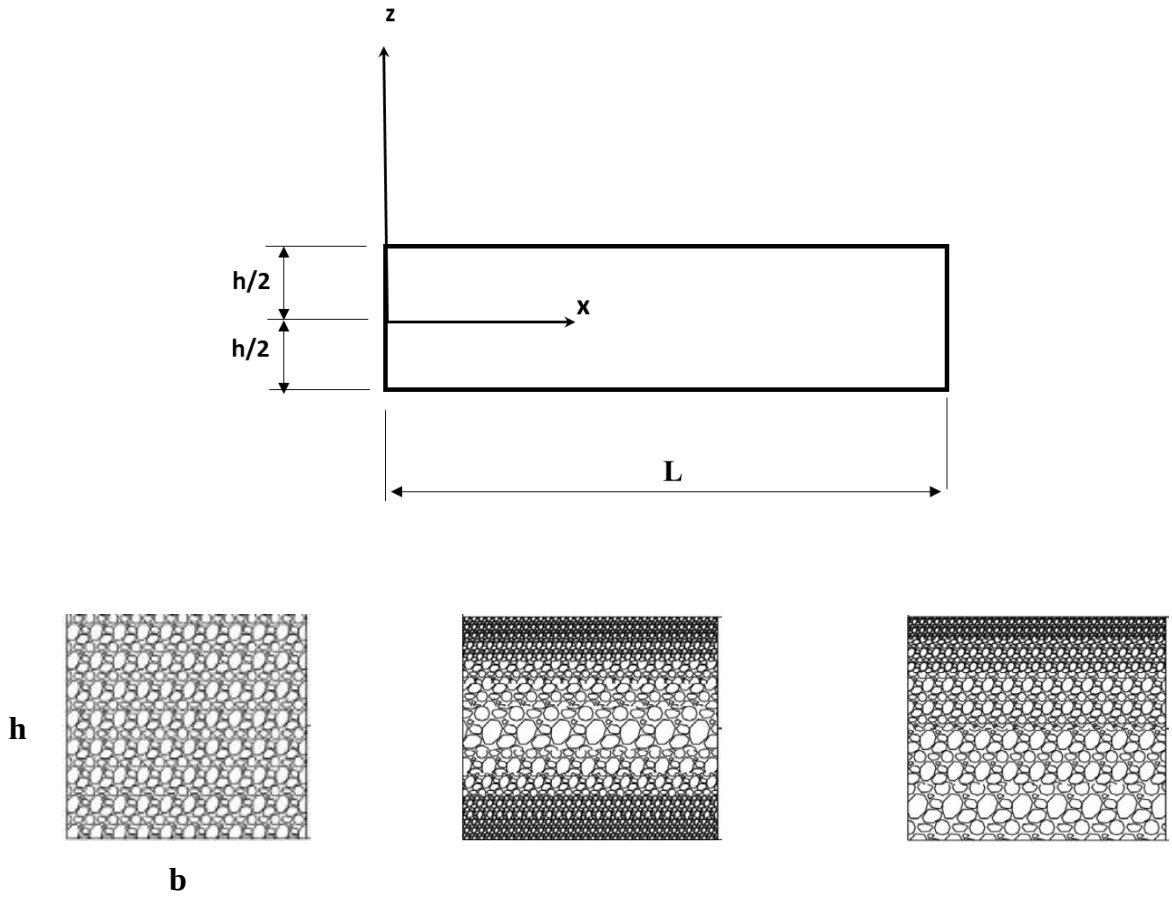


Figure 1. Metal foam porosity models

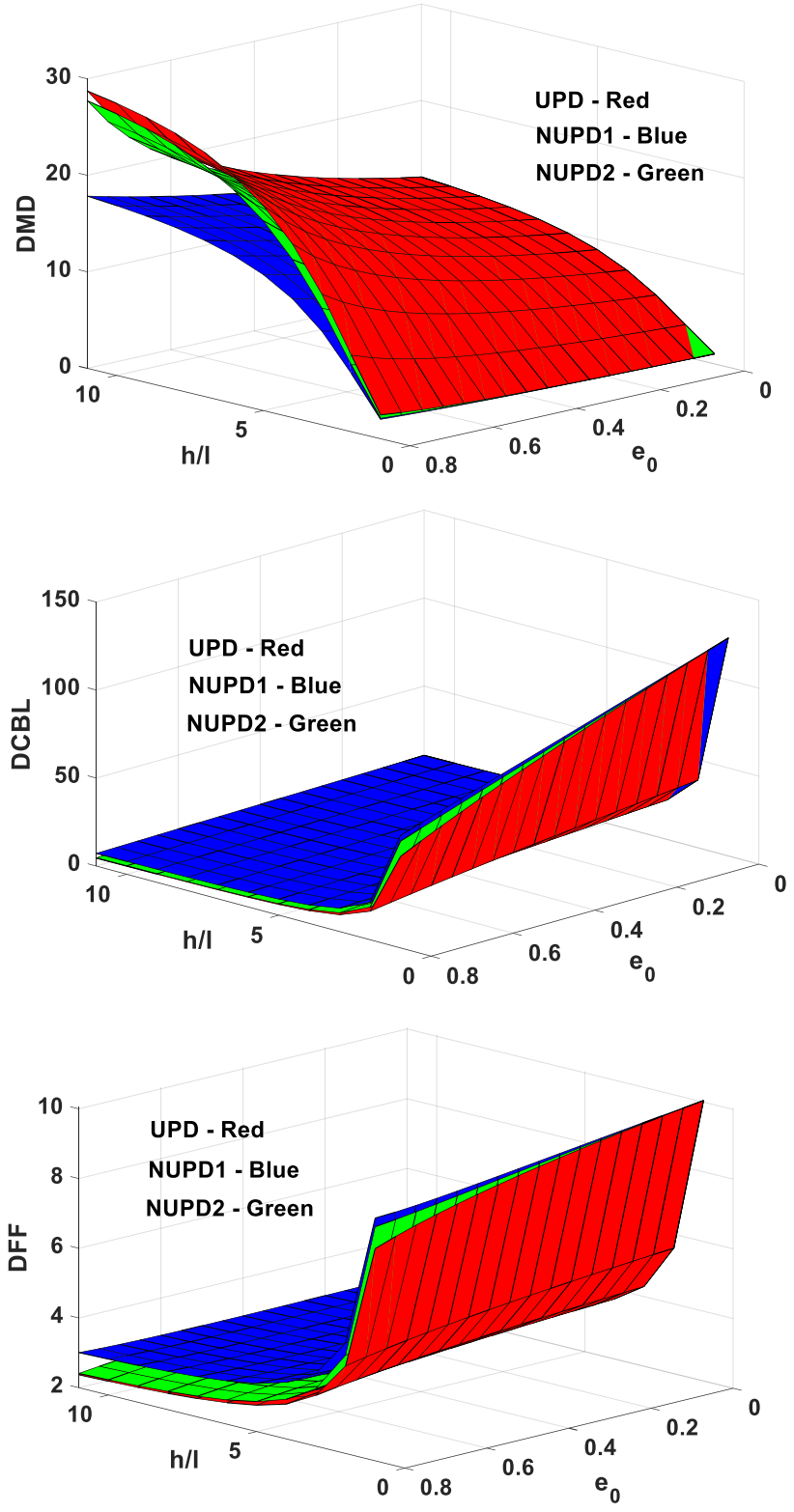
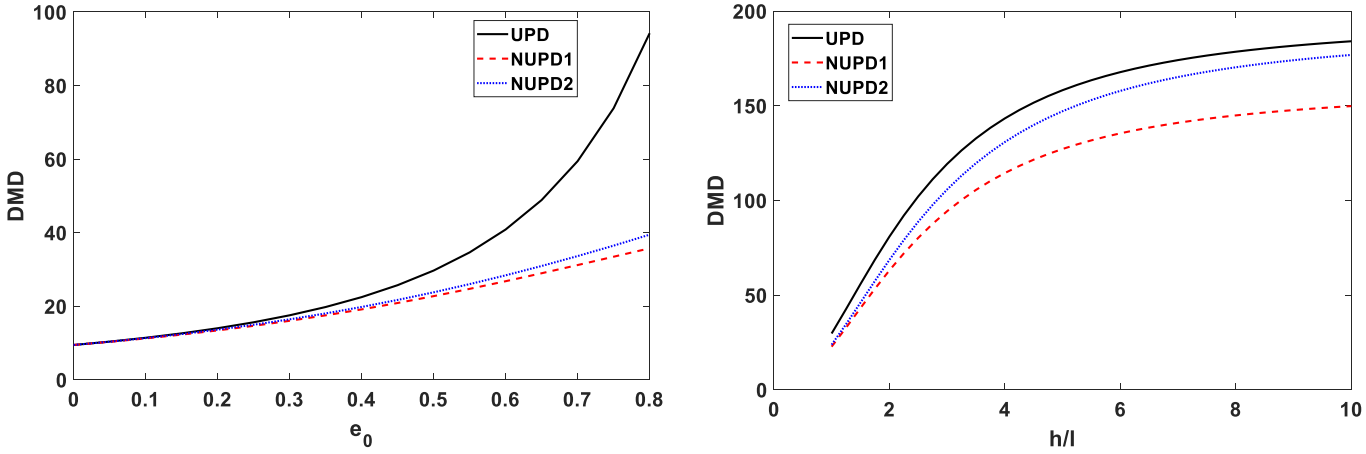
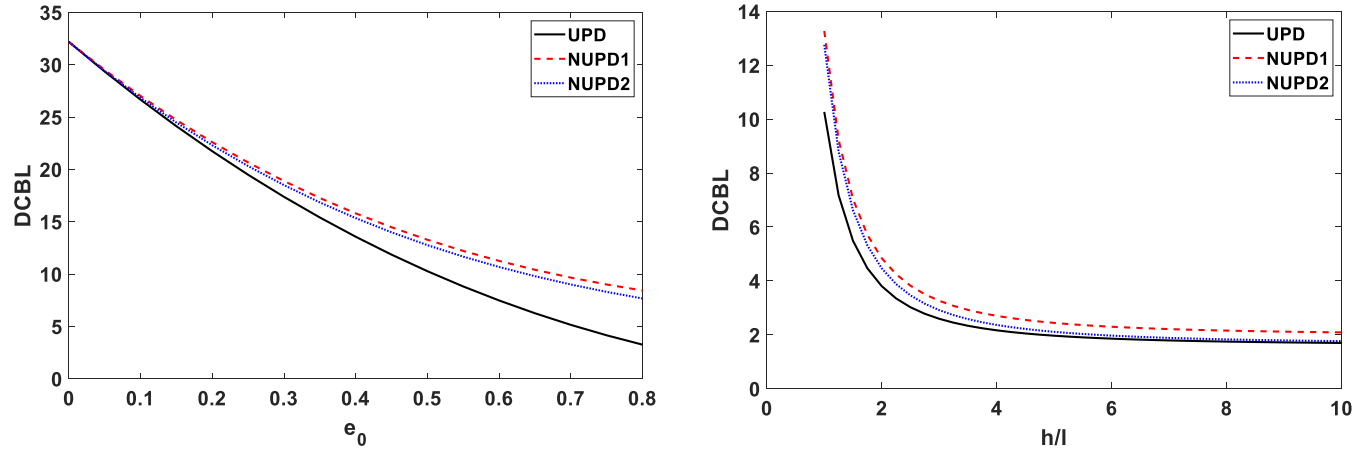


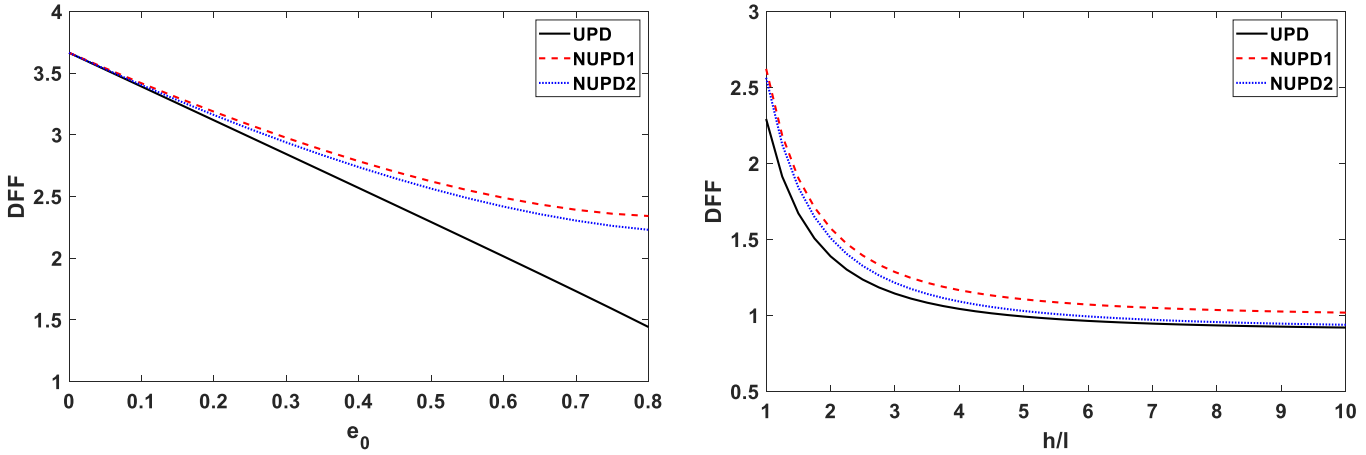
Figure 2. The results of S–S metal foam microbeams with respect to e_0 and h/ℓ ($L/h = 10, \ell = \ell_{max}$)



a) DMDs

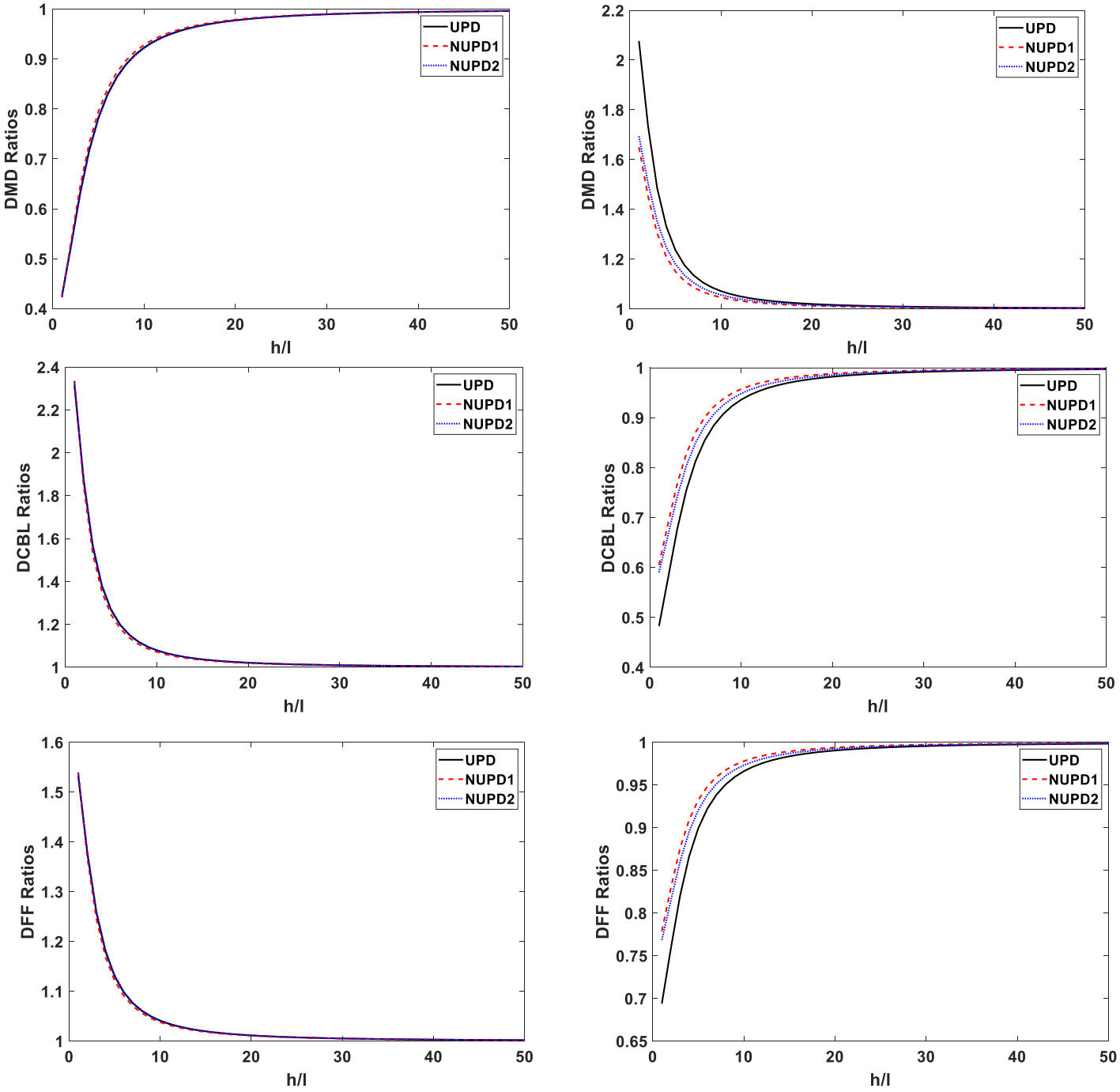


b) DCBLs



c) DFFs

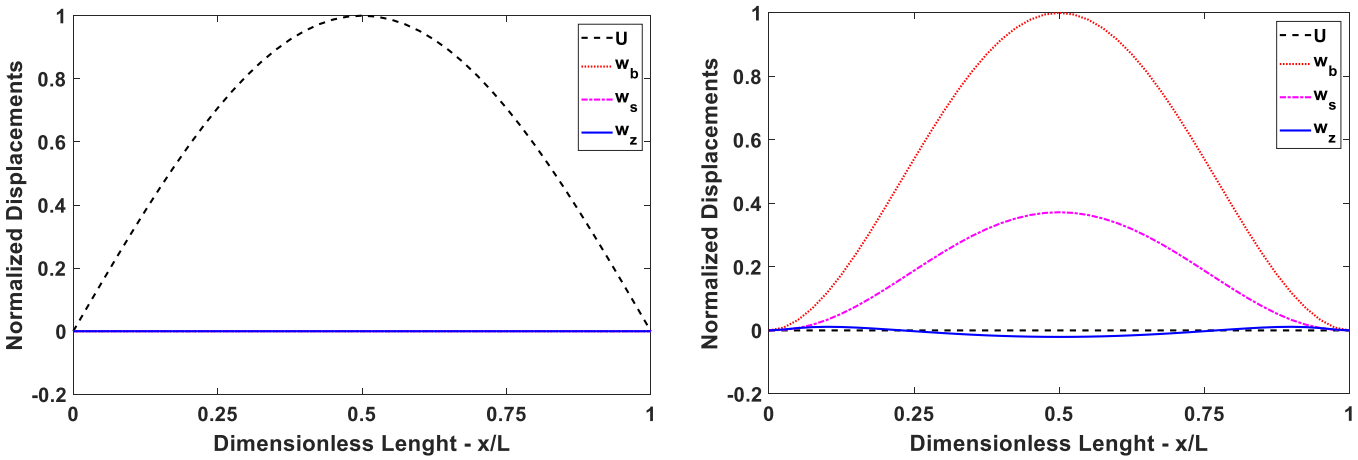
Figure 3. The results of C-F metal foam microbeams from MSGT obtained from variable MLSP with respect to e_0 $(L/h = 5, e_0 = 0.5)$



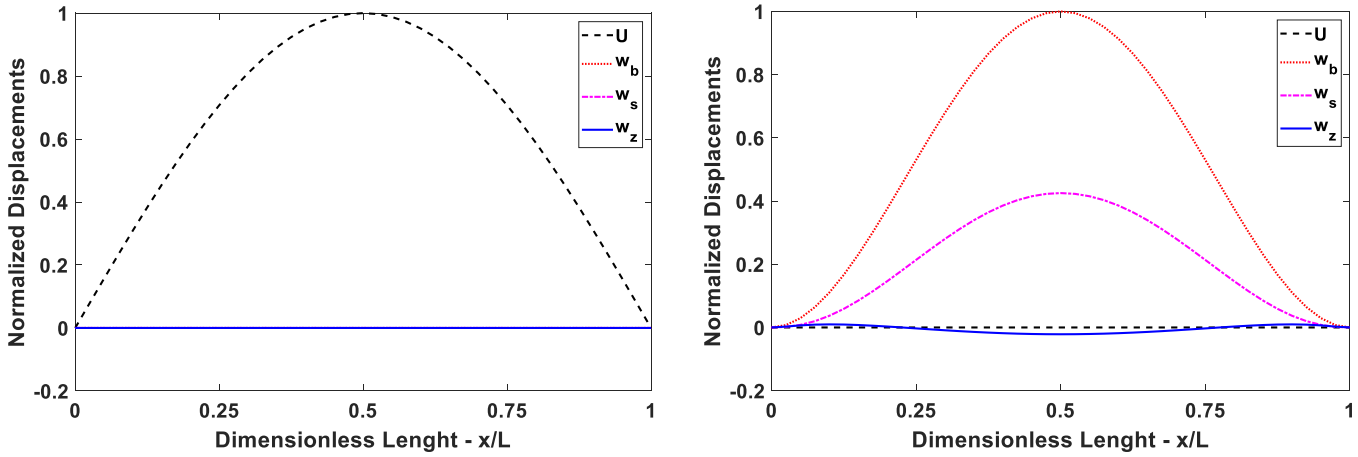
a) Ratios between MSGT and MCST

b) Ratios between variable and constant MLSP – MSGT

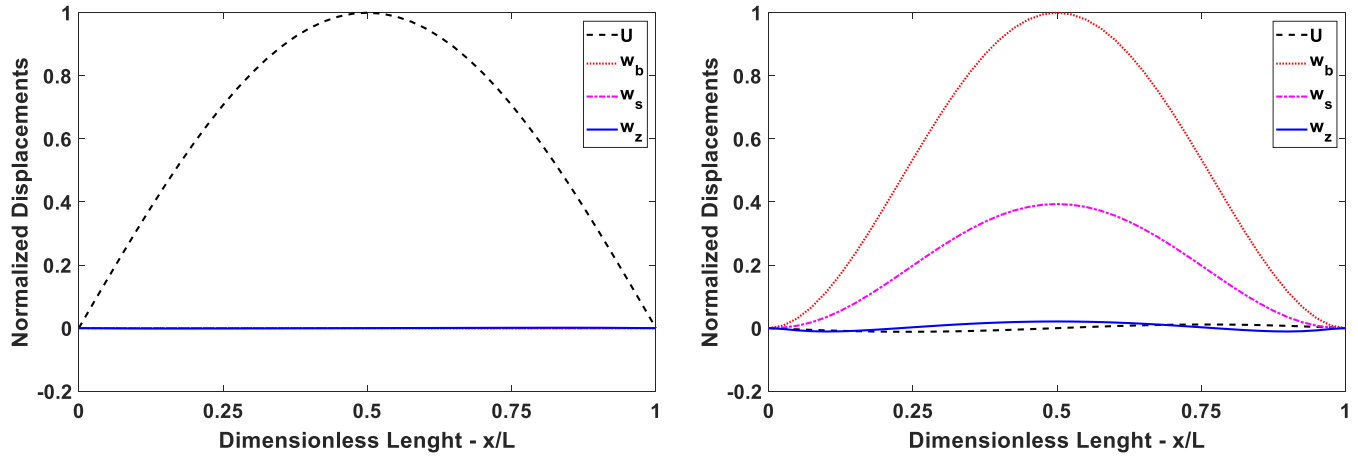
Figure 4. The results ratios of C-C metal foam microbeams between MSGT and MCST and those between variable and constant MLSP with respect to h/ℓ $(L/h = 10, e_0 = 0.5)$.



a) UPD



b) NUPD1



c) NUPD2

$\ell = \ell_{max}$ $\ell \neq \ell_{max}$

Figure 5. The fundamental vibration mode shapes of C-C metal foam microbeams ($e_0 = 0.5, h/\ell = 1, L/h = 10$)